TRIBHUVAN UNIVERSITY

INSTITUTE OF ENGINEERING

PULCHOWK CAMPUS

Biomass Derived ZnO/Carbon Composite for Wastewater Treatment

by

Charu Gajurel

A THESIS

SUBMITTED TO

DEPARTMENT OF APPLLIED SCIENCES AND CHEMICAL ENGINEERING

IN PARTIAL FULFILLMENT OF THE REQUIREMENTS FOR THE DEGREE OF

MASTER OF SCIENCE IN MATERIAL SCIENCE AND ENGINEERING

DEPARTMENT OF APPLLIED SCIENCES AND CHEMICAL ENGINEERING

LALITPUR, NEPAL

MAY, 2026

COPYRIGHT

APPROVAL PAGE

TRIBHUVAN UNIVERSITY

INSTUTE OF ENGINEERING

PULCHOWK CAMPUS

DEPARTMENT OF APPLIED SCIENCES AND CHEMICAL ENGINEERING

The undersigned certify that they have read, and recommended to the Institute of Engineering for acceptance, a thesis report entitled **"Biomass Derived ZnO/Carbon Composite for Wastewater Treatment"** submitted by Charu Gajurel in partial fulfilment of the requirements for the degree of Master of Science in Material Science and Engineering.

Supervisor, Dr. Tanka Mukhiya
Assistant Professor
Department of Applied Sciences and Chemical Engineering

External Examiner, Dr. Chhabi Lala Gnawali
Assistant Professor
Assistant Campus Chief, Pulchowk Campus

Committee Chairperson, Prof. Dr. Sahira Joshi
Head of Department
Department of Applied Sciences and Chemical Engineering

Date

ABSTRACT

Azolla Pinnata, a fast-growing aquatic fern with high nitrogen content was used as sustainable biomass template to grow ZIF-8 on it so as to use it to obtain ZnO/carbon composite through carbonization for removal of methylene blue (MB) dye from water. The zinc incorporated azolla biomass powder was carbonized in inert nitrogen atmosphere at three temperatures – 650 ˚C, 750 ˚C and 850 ˚C respectively. After that, it was heated in air environment which resulted into ZnO/carbon composites. The performance 10 mg each, of these ZnO/carbon composites were then evaluated for removal of MB dye from a 50 mL solution at initial concentration of 10 ppm over 120 minutes under UV. Samples carbonized at lower temperatures (650˚C and 750˚C) showed very poor adsorption and photocatalytic degradation. The 850˚C sample, however resulted in strong adsorption of 51.49 % and strong photocatalytic degradation with reduction in MB absorbance peak by 91.58 %. The better performance of ZnO/carbon composite carbonized at higher temperature can be attributed to formation of hierarchical pores that assisted in adsorption and better graphitization of the carbon matrix which increased the electron-hole separation at the ZnO sites during UV irradiation. This helped in ample formation of ROS for MB degradation. These findings are in agreement with studies on biomass-derived ZnO-carbon composites for dye removal.

Keywords: Azolla biomass, ZnO-carbon composite, methylene blue, adsorption, photocatalytic degradation

ACKNOWLEDGEMENTS

I would like to thank Institute of Engineering for providing me an opportunity to gain practical knowledge in the field of Material Science and Engineering by incorporating this thesis work in the curriculum of final year of M.Sc. of Material Science and Engineering. I would like to thank my supervisor Asst. Professor Tanka Mukhiya, PhD, IOE Pulchowk Campus for guiding me and providing assistance in every step of this project work. I would also like to express my gratitude to Asst. Professor Khem Raj Shrestha, PhD, IOE Pulchowk Campus, Asst. Professor Chhabi Lal Gnawali, PhD, IOE Pulchowk Campus, Asst. Professor Deval P. Bhattarai, PhD, ASCOL and Asst. Professor Purnima Mulmi, IOE Pulchowk Campus for guiding me and providing me assistance with various equipment in laboratory and other insights which were highly beneficial for this project. I would also like to thank Professor Sahira Joshi, PhD, Head of Department, Department of Applied Sciences and Chemical Engineering, IOE Pulchowk Campus, Assoc. Professor Ganesh Kumar Shrestha, PhD, Co-Ordinator, Material Science and Engineering program, Department of Applied Sciences and Chemical Engineering. My special gratitude to my colleague Mr. Bibek Ghimire, Department of Applied Sciences and Chemical Engineering, IOE Pulchowk Campus for his guidance and assistance in preparation of samples. Also, many thanks to my colleague Bipana Ojha Khatri, Department of Applied Sciences and Chemical Engineering, IOE Pulchowk Campus for being of great help throughout the course of this study.

TABLE OF CONTENTS

LIST OF ACRONYMS AND ABBREBIATIONS

$.O^{2-}$	- superoxide radical
.OH	- hydroxyl radical
AMR	- antimicrobial resistance
AOP	- Advanced oxidation process
APB	- azolla pinnata biomass
As	- arsenic
BDC	- biomass derived carbon
BPA	-bisphenol A
CA	- carbon aerogel
CB	- conduction band
Cd	- cadmium
CNT	- carbon nanotube
CO_2	- carbon dioxide
CQD	- carbon quantum dot
Cr	- chromium
Cu	- copper
CuO	- copper oxide
CW	- Constructed wetlands
DEWATS	- Decentralized Wastewater Treatment System
DW	- distilled water

e^- - free electron

EDS - Energy Dispersive Spectra

Fe_2O_3 - iron oxide (ferric oxide)

FeSEM - Field emission Scanning Electron Microscopy

FTIR - Fourier Transform Infrared Spectroscopy

GO - graphene oxide

H_2O - water

Hg - mercury

HTC - hydrothermal carbonization

KOH - potassium hydroxide

MF - microfilter

Mn - manganese

MO - methyl orange

MOF - metal organic framework

MWCNT - multi-walled carbon nanotube

N - nitrogen atom

N_2 - nitrogen gas

NF - nanofilter

NH^{4+} - ammonium ion

NP - nanoparticles

Pb - lead

pH - potential of hydrogen

PPCP - pharmaceuticals and personal care products

$R - NH^{3+}$ - protonated primary amine

RhB - Rhodamine Blue

RO - reverse osmosis

ROS - reactive oxygen species

SO_4^{2-} - sulphate ion

SSA - specific surface area

SWCNT - single walled carbon nanotube

TiO_2 - titanium dioxide

UF - ultrafilter

US - United States

UV - ultraviolet

VB - valence band

WWTP - waste water treatment plant

XRD - Xray Diffraction

ZIF - Zeolitic Imidazolate Frameworks

Zn - zinc

$Zn(NO_3)^2$ - zinc nitrate

Zn/MNC - zinc/magnetic nanocomposite

$ZnCl_2$ - zinc chloride

ZnO - zinc oxide

ZnO/C - zinc oxide- carbon composite

LIST OF SYMBOLS

%	- percentage
μm	- micrometer
cm	- centimeter
eV	- electron volt
g	- gram
gL^{-1}	- gram per litre
h	- hour
M	- mole
mg	- milligram
mL	- millilitre
$molL^{-1}$	- mol per litre
nm	- nanometer
ºC	- degree Celsius
ppm	- parts per million
W	-watt

LIST OF FIGURES

LIST OF TABLES

CHAPTER ONE: INTRODUCTION

1.1 Background

Water is a critical component for life on earth. Though 70 % of the earth's surface is covered with water, only 3 % of it is fresh water Bodzek et al. (2020). Moreover, only 1 % of this fresh water is available to humans for use. Rest of it is locked up in ice-caps, glaciers and groundwater. Currently over two-thirds of human population worldwide is facing water crisis (Mutegoa, 2024) which shows water is an essential yet, a scarce resource that needs to be managed wisely. With rapid industrialization, modernization of agriculture and livestock farming, and haphazard urbanization, especially in lesser developed countries, wastewater management has emerged as a significant challenge leading to rampant pollution of pristine water bodies like rivers, ponds, lakes, etc. In low-income countries, such as Nepal, there is a severe lack of resources. Such countries also suffer from the absence of stringent waste management regulations and sound strategies. Of approximately 359 billion m^3/year of total wastewater produced globally, 80 % is released into pristine water bodies without proper treatment(Karki et al., 2024).

Figure 1: Municipal wastewater being dumped directly into the Rudramati river, a tributary of Bagmati river in Kathmandu resulting in extreme water pollution

Household contribution to this wastewater not treated properly before being dumped is 42%. Most of this dumped wastewater belongs to low-income countries (unwater.org). This has resulted in extremely polluted rivers, ponds and lakes in urban areas of such countries. For

example, the Holy River, Bagmati and its tributaries which were the cradle of Kathmandu Valley civilization have within a few decades turned into sewer lines of Kathmandu city (**Figure *1***). The Fewa Lake which adorns the tourist destination of Pokhara Valley is rapidly shrinking due to invasion of water hyacinth caused by nutrient pollution due to dumping of the sewage of the city directly into it. Water pollution has become a major cause in loss of aquatic biodiversity. Also, various water borne diseases like cholera, typhoid, hepatitis A, E, diarrhoea and other serious health issues like cancer, neurological dysfunctions, endocrine disruptions, antibiotic resistance, etc. have become common in human population due to use of such polluted water. Polluted water bodies have caused negative impact on aquatic and migratory birds as well.

Wastewater primarily consists of municipal wastewater from household and institutional use, faecal sludge, industrial effluents and runoffs from farmlands. In addition to these sources, mining, oil drilling, air pollution, radioactive sources and landfill sites also cause water pollution. More than 1500 water pollutants have been identified so far. Among them, the major pollutants are large or suspended organic/inorganic residues, heavy metal ions such as Pb^{2+}, Hg^{2+}, Cd^{2+}, As^{3+}/As^{5+}, Cr^{6+}, Cu^{2+}, Ni^{2+}, etc., dyes, nutrients such as nitrates and phosphates, pesticides, pharmaceutical and personal care products (PPCPs), oil and microplastics, viruses and microbial pathogens, and other various toxic organic compounds like phenols and formaldehydes (Mitiku, 2020). Often wastewater treatment plants (WWTPs) use a combination of physical, chemical or biological methods for wastewater treatment. Physical treatments include screening, sedimentation, filtration, granular-medium, etc. Similarly, coagulation, chemical precipitation, ion exchange, chlorination, etc. fall under chemical treatment methods. The biological methods of wastewater treatment such as aerobic/anaerobic digestion, activated sludge process, constructed wetlands, stabilization ponds, etc. are mostly eco-friendly and sustainable though they can be slow and may occupy large areas (Karki et al., 2024).

The wastewater has to be passed through multiple stages of treatment before it becomes safe enough to be discharged into water bodies. In the preliminary stage, large objects like rags, plastics and other debris present in wastewater are removed. Then, during the primary treatment, all suspended and settleable organic and inorganic residues are separated by various

means ranging from sedimentation to coagulation or precipitation. After that, in the secondary treatment stage, most of the organic and inorganic compounds and various pathogens present in the wastewater are removed or their concentration is reduced to permissible limits. Generally, the treated water produced from this stage is then released into the environment and is clean enough for irrigation, flushing toilets, etc. However, even after secondary treatment, many micropollutants like dyes, heavy metal ions, PPCPs, pesticides, microplastics, viruses and pathogens, etc. remain in the treated water. These micropollutants are difficult to remove because they are ultra-small in size, chemically stable and non- biodegradable. To purify the treated wastewater from these recalcitrant micropollutants, it requires yet another tertiary level of treatment. Various methods like microfiltration (MF), nanofiltration (NF), ultrafiltration (UF), reverse osmosis (RO) and advanced oxidation processes (AOPs) such as UV irradiation, ozone treatment, electrochemical oxidation, photocatalytic degradation, etc. have been developed to deal with such micropollutants (Amin et al., 2014) ; (Manna & Sen, 2023).

In developed countries like the US, Japan and others, strict regulations and well-managed wastewater disposal and treatment systems are in place. At least, secondary level treatment is performed on the wastewater before it is released into the environment. Large centralized WWTPs as well as smaller decentralized units are used to clean wastewater. “Jokhasou” is an example of such a decentralized single-home water treatment unit popular in rural Japan. It can clean up both “black water” (fecal sludge) as well as “grey water” (kitchen, bath/laundry discharge) using aerobic, anaerobic digestions and microfiltration/ disinfection in a three-chamber unit (Asian Development Bank, 2021). In low-income countries, more sustainable and inexpensive physio-chemical or biological methods like coagulation, flocculation, activated sludge process, constructed wetlands (CWs) are used for wastewater treatment. In Nepal, centralized WWTPs are only a handful as given in **Table *1***. CWs have been more popular in Nepal in semi-urban municipalities and in hospitals as well (Karki et al., 2024).

Whether in the advanced high-income countries or in the lesser developed world, the main challenge in wastewater treatment lies in cleaning up of the micropollutants from the wastewater. As we discussed earlier, many methods of filtration like the MF, NF, UF and RO have been devised to clean up micropollutants still present in the treated wastewater. However, these methods are highly expensive and the filtration membranes used are prone to bio-fouling.

Also, the captured pollutants are not degraded, but just separated, so the challenge of degrading and mineralizing them still remains. AOPs can overcome this challenge by effectively degrading the micropollutants. But the AOP methods such as UV irradiation, ozone treatment and electrochemical oxidation are costly and difficult to scale up.

Name of the project	Location	Type of treatment system	Types of treatment plant	Treatment capacity (MLD)	Status	Responsible organization
Guheshwori wastewater treatment plant	Guheshwori, BP	Biological	Activated sludge process	32.4	Functional	KUKL
Sallagahri, Kodku, and Dhobighat wastewater treatment plant	Sallagahri, Kodku and Dhobighat, BP	Biological	Activated sludge process	14.2, 17.5, and 37	Construction phase	KUKL
Dhobighat wastewater treatment plant	Dhobighat, BP	Biological	Activated sludge process	37	Construction phase	KUKL
DEWATS at Gokarna and Hanumanghat	Gokarna and Hanumanghat, Bhaktapur, BP	Biological	Membrane-based biological reactor	1 and 3	Design phase	KUKL
Birgunj wastewater treatment plant	Birgunj, MP	Biological	Waste stabilization pond	10	Functional	STIUEIP (Birgunj Metropolitan)
Biratnagar wastewater treatment plant	Biratnagar, KP	Biological	Waste stabilization pond	18.5	Functional	STIUEIP (Biratnagar sub-metropolitan)

Table 1: WWTPs currently active, under construction or in design phase in Nepal (Karki et al., 2024)

Nanomaterials have particularly gained interest in water remediation processes because their size corresponds to the size of the recalcitrant micropollutants that we intend to remove in the advanced tertiary level of water purification. The materials that escape traditional filtrations and other methods can be targeted by suitable nanoparticles even at very low concentrations. The problem of bio-fouling seen in MF, NF, UF membranes can be removed through their modification by attaching silver or silica nanoparticles on their surfaces. Excellent anti-microbial properties have been exhibited by silver, copper and iron nanoparticles. This anti-microbial property can thus be used to disinfect the water from harmful pathogens. Similarly, single walled carbon nano tubes (SWCNTs), multi-walled carbon nanotubes (MWCNTs) and graphene oxide (GO) can be used as adsorbents that can remove toxic metals and organic compounds from water selectively, but again, they cannot degrade the pollutants and their

synthesis process is complex and costly. Furthermore, there is a risk of the miniscule nanoparticles leaching into the purified water and entering living organisms and causing harmful effects as their toxicity to humans and animals in vitro and in vivo is not well established (Amin et al., 2014); (Epelle et al., 2022). Nanoparticles of metal oxides like titanium dioxide (TiO_2) and zinc oxide (ZnO) and carbon quantum dots (CQDs) can be used as photocatalysts to break down and mineralize complex dyes, pharmaceutical products and pesticides into water (H_2O) and carbon dioxide (CO_2) in the presence of ultraviolet (UV) light (Bekele & Alamnie, 2025). Magnetic photocatalysts with ferromagnetic oxides in them too have been synthesized and studied for removal of recalcitrant organic and aromatic compounds from water. They are seen to have great efficacy and they can be fully recovered and recycled by simply using a magnet to fish them out of water (Ibrahim et al., 2022). The photocatalytic nanoparticles of metal oxides such as TiO_2 are effective but costly and those such as ZnO, CuO, Fe_2O_3 etc., and also the CQDs suffer from the drawbacks of agglomeration and quick recombination of electron-hole pairs formed during UV irradiation.

Single component photocatalysts suffer from a grave problem of quick electron-hole recombination that reduces their efficiency considerably. Therefore, metal oxide heterojunctions were engineered to move the electron- hole pair generated by the light photon on the metal oxide surface far apart from each other so that they get ample time to react with dissolved oxygen and water to form ROS. Various structured nanoparticles or surfaces have been designed using different types of heterojunctions such as Type I, Type II, Z-scheme, S-scheme and p-n junction which have been able to optimize the photocatalytic potentials of these materials. Such heterojunctions can be built using semiconductor-semiconductor composites, metal-semiconductor composites or carbon-material composites (Bekele & Alamnie, 2025). Metal oxide heterojunctions face some significant challenges like lattice mismatch and increased interfacial resistance due to poor bonding between two materials. In ZnO/TiO2 systems, ZnO shows a tendency to leach into water under light exposure. During high-temperature synthesis, the two semiconductor oxides instead of forming heterojunction interface may react to form an inactive third phase such as formation of Zn2TiO4 instead of ZnO/TiO2 (Low et al., 2017). Metal oxide - carbon composites have been found to be more effective as the metal oxides and the carbon matrix elements exhibit synergistic effect on each other in such a way that they do not suffer from the challenges like other composites. It has

been found that since photocatalysts can degrade and mineralize pollutants while carbon matrices can effectively adsorb and bind the pollutant molecules onto their surfaces, their combination can create the synergy that overcomes the drawbacks they face single-handedly. Therefore, the AOP method of photocatalysis with major modification via composite formation with biomass derived carbon (BDC) matrix promises to be an easy, cost-effective as well as scalable method for degradation of micropollutants. Semiconductor materials can be engineered to be grown on BDCs to form composites such that their photocatalytic performance will be greatly enhanced by the synergy between these two materials.

The BDCs used for photocatalysis are synthesized mainly by two approaches, bottom-up or top-down. In bottom-up approach hydro-soluble carbohydrates are used as precursors and are carbonized by hydrothermal carbonization (HTC) in controlled environments to derive nanocomposites while in top-down approach biomass sources are directly taken as precursors which are then surface-modified either by activation or incorporation of active materials like MOFs, etc. followed by carbonization. The top-down approach has the benefit of being low-cost, simple to fabricate and shows promise for scaling up (Zhang et al., 2026). Metal oxide/ activated carbon (AC) composites have been a popular top-down method in photocatalytic degradation studies because of high adsorption capacity of its carbon matrix and good enough photocatalytic activity exhibited by the composites for both visible and UV light (Kumari, 2022), (Shintre et al., 2022), (Salah et al., 2024). However, their largescale application has been prevented due to some serious limitations. If the carbon content is too high, it shields and blocks the light photons from reaching the metal oxide sites. Similarly, the metal oxide nanoparticles can physically block the carbon matrix pores, reducing the effective surface area available for adsorption. Also, metal oxide particles can get buried under the carbon matrix itself. Furthermore, metal oxides like ZnO, under light exposure in aqueous environment become unstable and leach into the water as metal ions. This happens because the metal oxide-carbon bonds are not strong enough in the composite. Also, it is very difficult to uniformly distribute the metal oxide nanoparticles over the AC surface. The metal oxide particles tend to aggregate during carbonization, thereby reducing the photocatalytic sites (Andriantsiferana et al., 2014).

These problems observed in metal oxide/AC composites can be tackled by using metal organic frameworks (MOFs) instead. MOFs can be grown on the biomass substrate and then carbonized in inert atmosphere. MOF will act as a sacrificial template and since MOFs have metal nodes linked by organic linkers, upon carbonization, metal atoms get separated from each other at the molecular level itself preventing their aggregation. Moreover, metal oxide is formed simultaneously along with the carbon matrix during the process of carbonization. This ensures that the active metal oxide sites are distributed evenly throughout the matrix surface. Also, the strong chemical bond between the metal ion and organic linkers is preserved even after carbonization so the metal oxide gets strongly bound to the carbon matrix. This eliminates the problem of leaching of metal ions into the aqueous environment upon exposure to light. Also, MOFs already have high porosity and surface area. So, upon carbonization their micro and mesopores remain intact which will be further linked with the macropores of the carbon matrix increasing the surface area for adsorption of the pollutants (Hussain et al., 2019).

In this study, we aim to synthesize an MOF called Zeolitic Imidazolate Framework – 8 (ZIF-8) on *azolla pinnata* biomass which upon carbonization under inert atmosphere yields ZnO/carbon composite. The efficacy of this as-synthesized ZnO/C composite is then studied for photocatalytic degradation of micropollutants using methylene blue (MB) dye as the model pollutant. Since ZIF-8 is thermally stable till 550 ˚ C (Bergaoui et al., 2021) and vapourization temperature under inert conditions for Zn is 907 ˚C(Hussain et al., 2018) , we will attempt to study the performance of the ZnO/C composites hence derived at three carbonization temperatures of 650 ˚C, 750 ˚C and 850 ˚C.

1.2 Photocatalytic degradation - A green technology

Among various methods of tertiary treatment of wastewater, photocatalytic degradation has emerged as a superior "green" advanced oxidation process. It completely destroys and mineralizes the complex aromatic compounds into CO_2, H_2O and mineral acids leaving no intermediates by generating highly reactive oxygen species (ROS) under light exposure. Unlike other methods such as filtration and adsorption, it does not just move the pollutants from one phase to another. It creates ROS like hydroxyl radical (**.**OH) that can attack a wide range of pollutants ranging from complex compounds with aromatic rings to bacteria and heavy metal ions. Photocatalytic degradation works under ambient conditions and requires no

special thermal or high-pressure environment, thus saving energy. It does not require hazardous chemicals like chlorine or ozone. Photocatalytic materials can be designed to harvest even visible light such that it can function efficient under natural lighting conditions. Incorporating magnetic components into the photocatalyst makes the photocatalyst easily recoverable and reusable (Al-Nuaim et al., 2023). TiO_2, ZnO, CuO, Fe_2O_3 etc are some metal oxides that have been widely used as photocatalysts. Since we are growing ZIF-8 MOF on the biomass substrate, ZnO will be the photocatalytic component in this study.

Zinc oxide as photocatalyst. Pure ZnO is a semiconductor with a bandgap of 3.2 to 3.37 eV. It shows good photocatalytic activity under UV light. On exposure to UV light, electrons in the valence band (VB) of ZnO will jump to the conduction band (CB) producing electron-hole pairs. These electrons and holes will separately interact with oxygen dissolved in water or with water itself to produced reactive oxygen species (ROS) like superoxide anions (**.**O_2^-) and hydroxyl radicals (**.**OH) (**Figure *2***).

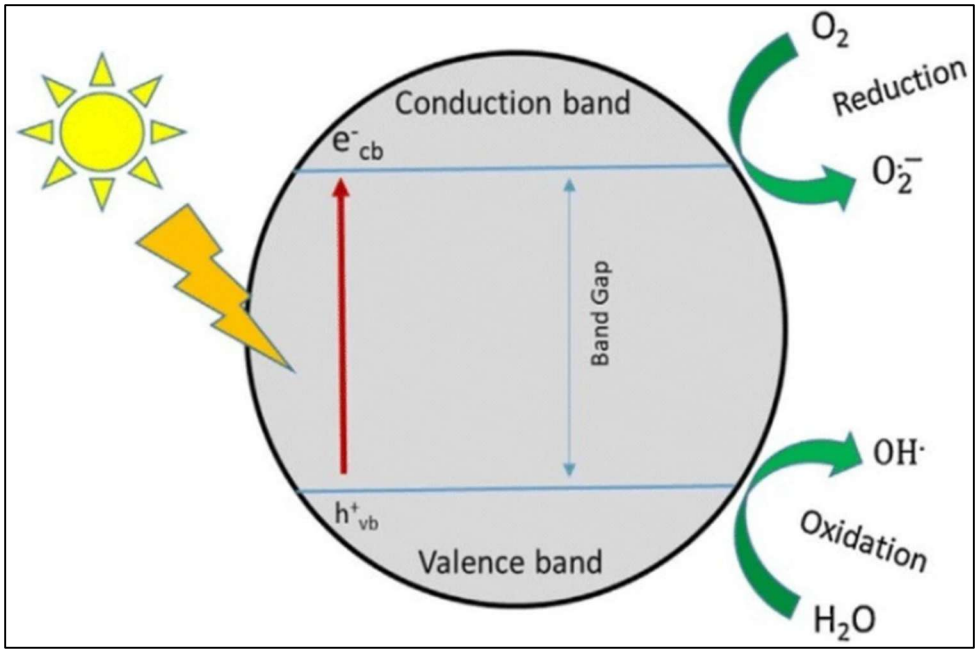

Figure 2: Mechanism of generation of ROS through photolytic process by ZnO (Isai & Shrivastava, 2019)

These ROS have the capacity to oxidize and mineralize organic pollutants like dyes, to destroy microbes and to help capture heavy metal pollutants. However, pure ZnO has some drawbacks.

It suffers from rapid electron-hole recombination, nanoparticle aggregation, photo corrosion and very little response to visible light. Also, it is difficult to recover the material back from the aqueous suspension causing a problem of leaching (Hu et al., 2020). ZnO-carbon composites however have been found to overcome these limitations very effectively.

1.3 Zinc oxide - carbon composites

ZnO-carbon composites are a class of advanced functional materials that combine the photocatalytic activity of ZnO nanoparticles with adsorptive properties of carbon matrix derived from biomass or activated carbon. The carbon matrix provides high surface area and porosity which helps to uniformly distribute ZnO nanoparticles on the carbon surface removing the problem of aggregation. Most importantly, the carbon matrix acts like a electron sink, thus removing the electron-hole pair recombination problem seen in pure ZnO. Furthermore, the N-doping of carbon matrix composite formation allows for the bandgap to narrow down to visible light range. Also, the carbon matrix prevents photo corrosion of ZnO and allows reusability. The synergistic effect of adsorption of pollutants on carbon matrix surface near the ZnO nanoparticles and photocatalytic action of ZnO nanoparticles on these trapped pollutant molecules make ZnO- carbon composites superior to pure ZnO nanoparticles (Cruz et al., 2018). Biomass derived carbon (BDC) matrices have the advantage of being low-cost, having high nitrogen-content for N-doping, presence of lignocellulose and various functional groups resulting in higher porosity and surface area for ZnO to distribute over (Zhang et al., 2026). Researchers have attempted to investigate many biomass sources like corn cobs (Cruz et al., 2018), banana peels (Eswaran et al., 2025), peanut shells (Ilhami et al., 2024), (Darabdhara et al., 2026; Thi Luyen et al., 2023), cauliflower leaves (Darabdhara et al., 2026), aloe vera (Chander et al., 2024), bacterial cellulose (Ma et al., 2025) etc. as cheap and sustainable sources of carbon matrix for ZnO-carbon composites. In fact, any biomass waste ranging from agricultural residue, animal manure to food and kitchen waste can be repurposed as valuable carbon source with each having their specific advantages and disadvantages (Zhu et al., 2025). Various methods have been developed for synthesis of biomass derived ZnO-carbon composites. BCDs used for photocatalysis are synthesized mainly by two approaches, bottom-up or top-down. In bottom-up approach hydro soluble carbohydrates are used as precursors and are carbonized by hydrothermal carbonization (HTC) in controlled environments to derive

nanocomposites while in top-down approach biomass sources are directly taken as precursors which are then are surface modified either by activation or incorporation of active materials like MOFs, etc. followed by carbonization. The top-down approach has the benefit of being low-cost, simple to fabricate and shows promise for scaling up (Zhang et al., 2026). Some methods for synthesis of BDCs by top-down approach are as follows:

One-step pyrolysis: In this method, powdered biomass is directly mixed with Zinc precursors like $ZnCl_2$ or $Zn(NO_3)_2$ and pyrolyzed under inert or limited oxygen atmosphere to form porous carbon structure with well dispersed ZnO particles on it.

Impregnation followed by calcination: First biomass is converted into biochar and then is loaded with ZnO using Zn precursors and then heated.

MOF templated method: Zinc based MOFs are grown on the biomass and then controlled carbonization is done to produce uniformly dispersed N-doped carbon matrices. Growth of MOF structures results on higher porosity and surface area of the carbon matrix. Also, higher temperature carbonizations result in better graphitization of carbon matrix, superior crystallinity of ZnO particles and better interfacial contact between ZnO particles and carbon matrix. This method is superior to other two methods and is being actively researched currently (Cruz et al., 2018).

1.4 Zeolitic Imidazolate Framework – 8 (ZIF-8)

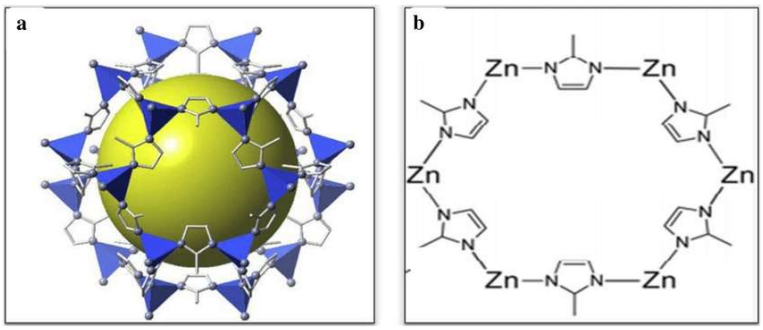

Figure 3 : a) ZIF-8: Zn (polyhedra), N (sphere), and C (line). The massive sphere represents the largest Van der Waals spheres that would fit in the cavities without touching the framework. (b) ZIF - 8 structure (Kouser et al., 2022)

Zeolitic imidazolate frameworks (ZIF) are a class of MOFs whose structure is similar to the structures of zeolites with large network of porous structures. ZIFs are formed by connecting four tetrahedral units in which metal ions like Zn^{2+} or Co^{2+} are linked through nitrogen atoms of imidazolate anions(Lee et al., 2015). ZIF-8 is formed through linking of Zn^{2+} ions with 2-methylimidazole linker and has a sodalite topology. It has large pore cage of 1.16 nm diameter which is connected through six membered window of size 0.34 nm (Lee et al., 2015); (Jian et al., 2015).

The morphology, crystal size and other surface properties of ZIF-8 are highly dependent on the synthesis conditions, concentrations and solvents used. Generally, organic solvents such as N,N dimethylformaimide (DMF), ethanol, methanol, etc. are used to synthesize nanoparticles of ZIF-8. However, organic solvents are flammable, expensive, toxic and not very environment-friendly. So, water-based facile synthesis methods have also been developed by which ZIF crystals can be grown. In water-based synthesis, 2-methylimidazole is first deprotonated with water and then is coordinated with Zn^{2+} to form ZIF-8. Though it is difficult to synthesize ZIF crystals with regular particle morphology in water medium without any supporting additives, in our case, however, as crystal defects in ZIF-8 grown in water medium ((Möslein et al., 2021); (Zhang et al., 2016)) are particularly useful to create larger pores upon carbonization, synthesis of ZIF-8 in aqueous medium is advantageous. As we have discussed earlier, the ZIF-8 window pores are only 0.34 nm in size, so the bulky MB dye molecules (1.69 nm × 0.74 nm × 0.38 nm) cannot enter into the internal cavity via normal diffusion. Thus, adsorption of MB dye occurs more through π-π stacking and less through diffusion into ZIF-8 pores (Jing et al., 2014). Crystal defects, thus can help to create larger pores for increasing MB adsorption. Also, ZIF-8 has been found to be thermally stable till 550 ˚C (Bergaoui et al., 2021).

1.5 Azolla pinnata biomass

Figure 4: (a) Azolla pinnata biomass (b) A. pinnata herbarium sample sent for identification (c) Certification of the same provided by National Herbarium and Botanical Laboratory, Godavari

Azolla pinnata is a fast-growing aquatic fern that is found growing in slow moving or still water bodies, as pictured in **Figure 4** It is also cultivated as poultry and fishery feedstock due to its high protein content. It is also used in rice-cultivation for nitrogen fixation because of its symbiotic relationship with nitrogen-fixing cyanobacteria *Anabaena azollae*. *Azolla pinnata* has a very high growth rate. Under optimal conditions of temperatures up to 30˚C and pH 6.5 -7.5 it can double in quantity within a short time duration of 2 to 5 days (Cary & Weerts, 1992). It can also be cultivated in the wastewater itself and is well known for its phytoremediation properties (Jayasundara, 2022).

Azolla pinnata is rich in proteins, nitrogen, cellulose, hemicellulose and pectin in its cell walls. High nitrogen content helps in natural N-doping of the carbon matrix during carbonization. N-doping results in narrowing of the ZnO bandgap making photocatalytic activity in presence of I ko visible light feasible. The lignocellulosic structure helps to create hierarchical porous carbon matrix with high surface area during carbonization and also helps to distribute ZnO uniformly in the matrix. Thus, azolla pinnata can act as a low-cost sustainable source of carbon matrix for ZnO-carbon composite aimed for synergistic adsorption and photocatalytic activity for various applications.

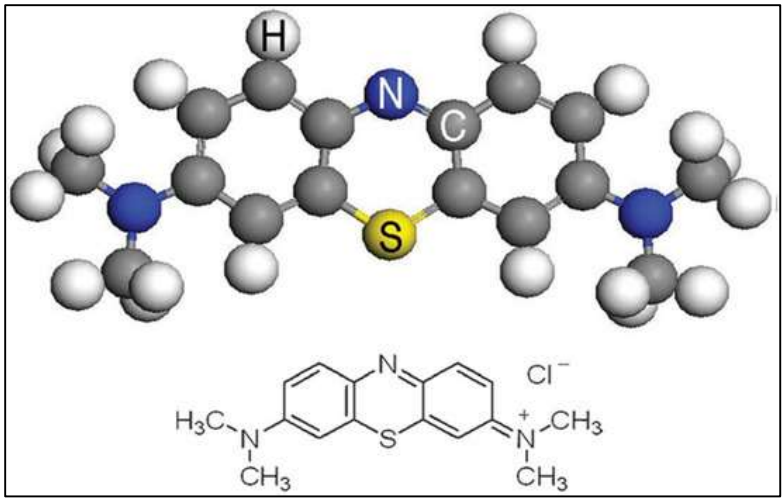

Figure 5: A Methylene blue molecule (I. Khan, et al)

1.6 Methylene Blue dye

Methylene Blue (MB) having chemical formula $C_{16}H_{18}ClN_3S$ is a cationic thiazine dye (**Figure 5**) which is commonly used in textile, paper, leather and pharmaceutical industries as a colouring agent. It is also popularly used as biological stain. MB is highly water soluble and chemically stable. It has an intense blue colour with strong absorption peak at 664-665 nm and a shoulder around 610-620 nm (Oladoye et al., 2022). Even at low concentrations, it prevents light from penetrating deeper water layers causing loss in photosynthetic capacity of aquatic plants and algae. It does not biodegrade easily and is toxic to humans at higher doses. It enters wastewater through laundry washing or textile industries. It is an excellent model pollutant for evaluation of advanced functional materials in water remediation (Khan et al., 2022)

The ROS $\cdot O_2^-$ and $\cdot$OH radicals are the ones responsible during photodegradation of MB. The degradation occurs through a series of steps. Firstly, demethylation occurs followed by scission of the MB ring. Then, the side aromatic rings are further broken down to produce intermediates like R-NH_3^+, phenols, aniline and aldehydic or carboxylate species. These intermediates are further acted upon by the $\cdot O_2^-$ and $\cdot$OH radicals and converted into aldehydes, carboxylic species, phenols and amines which are then finally degraded into H_2O, CO_2, NH_4^+ and SO_4^{2-} ions. The breaking up of the aromatic ring causes the aqueous solution of MB to lose colour (Khan et al., 2022) (**Figure 6**).

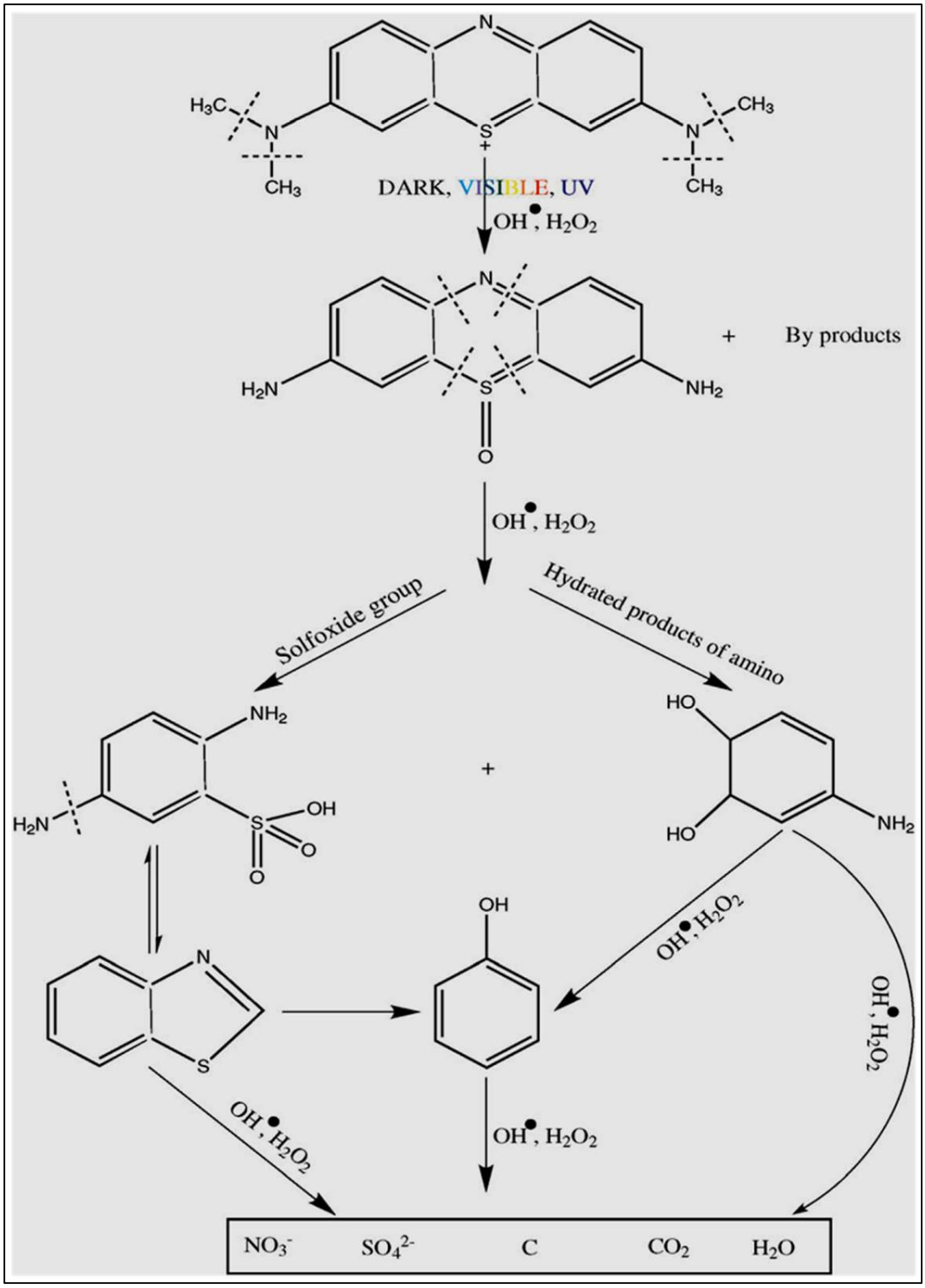

Figure 6: Reaction pathways of methylene blue degradation by ZnO photocatalysis (Khan et al., 2022)

1.7 Motivation

With increase in urbanization and industrialization worldwide, municipal and industrial wastewater management is becoming a major environmental challenge. Wastewater treatment remains costly and challenging mostly due to a large mix of pollutants found in it. Not a single method or single step treatment is able to solve the problem entirely. After removing solid residues and nitrogen or phosphorous rich compounds from the wastewater by primary and secondary water treatments, tertiary level cleaning is also needed to remove recalcitrant micropollutants like dyes, antibiotics, heavy metals and microplastics from it. So, advanced multifunctional materials that are sustainable, low cost as well as effective are urgently in demand. ZnO-carbon composites are such attractive materials which can through photocatalytic degradation completely mineralize even complex and recalcitrant organic aromatic compounds and even microbes. However, compared to AC composites, MOF based composites are expected to show better efficiency. The study of MOF derived metal oxide-carbon composites obtained from various biomass sources are still in initial phase. *Azolla pinnata*, a nitrogen fixing aquatic fern which grows very rapidly even in waste water itself can be used as a sustainable and cheap biomass source for this purpose. Also, synthesis of MOF on the biomass should be kept as simple, green and cheap as possible. Since the imidazole linker is costly, its cost must be offset by other means to keep the overall process cost-effective. Thus, this study aims to synthesize ZIF-8 MOF on azolla pinnata biomass substrate in aqueous medium, then carbonize it in inert atmosphere to produce ZnO-carbon composite. This hence obtained ZnO-carbon composite will then be studied for photocatalytic degradation of MB dye.

1.8 Research Gap

- MOF based ZnO-carbon composites have not been widely studied till date despite their theoretical potential in photocatalytic degradation.
- Though direct pyrolysis of MOFs has been done to obtain metal oxide – carbon nanocomposites, MOF has not been grown on biomass substrate as sacrificial template for ZnO-carbon composite formation after carbonization in inert conditions.
- Azolla pinnata biomass, despite of it being an easily available sustainable source of carbon, has not been used in metal oxide - composite studies using MOFs/ZIFs.

1.9 Objectives

General Objective

To prepare ZnO-carbon composite from azolla pinnata biomass using ZIF-8 and use this composite to remove methylene blue dye from water.

Specific Objectives

a) To grow ZIF-8 crystals on the azolla pinnata biomass in aqueous medium and ambient conditions.

b) To pyrolyze the as synthesized ZIF-8 integrated azolla-pinnata biomass at three carbonization temperatures of 650˚C, 750˚C and 850˚C.

c) To characterize the samples using FeSEM/EDS, FTIR and XRD to study the surface morphology of the composites, their elemental composition, formation and dispersal of ZnO particles in the carbon matrix.

d) To study the adsorption of MB dye molecules in the carbon matrix of the composite in dark.

e) To study the photocatalytic degradation of methylene blue by the ZnO-carbon composite under UV light exposure using UV source and UV vis spectrometer.

CHAPTER 2. LITERATURE REVIEW

Since the advent of nanotechnology, various nanomaterials have been explored to solve a wide range of problems from energy storage, carbon capture, drug delivery, sensor applications to water remediation. Nanomaterials have shown huge potential in wastewater treatment via their filtration, adsorption or degradation capabilities. Amin et al. (2014) reviewed the initial progress made in synthesis and application of nanomaterials for removal of pollutants from water/wastewater. They note emergence of nanoscale filtration techniques like MF, NF, UF, RO and antimicrobial properties of various nanoparticles (NPs) such as AgNP, CuNP, photocatalytic degradation of microbes by metal oxide NPs such as TiO_2, ZnO and CQDs. Similarly, carbon NPs like CNTs, nano fibres, graphene and GO sheets are appreciated for high adsorptive capacities and anti-microbial properties. Epelle et al. (2022) further reviewed the performance of nanomaterials such as various nanocomposite membranes used in MF, NF, UF, RO, CNTs, graphene, fullerenes, Ag, Cu NPs in water remediation and noted that though biofouling of membranes can be prevented by incorporation of anti-microbial NPs like Ag, SiO2 in the membranes, the pollutants are merely transferred. The pollutants still persist in the environment as they are not degraded. Similar problem is encountered with adsorbents like CNTs, graphene, GO, etc. Furthermore, their recovery is difficult and these NPs can leach into water and cause toxicity. Their synthesis is complex and costly. Another issue seen in carbon-based NPs is their hydrophobicity and tendency to agglomerate.

Kordbacheh and Heidari (2023) note that photodegradation method has a very good potential in water remediation technology because it can be used to remove pesticides, colours, pharmaceuticals and other organic compounds from wastewater by completely mineralizing them. No extra chemicals are required and the process can be performed in ambient conditions. Materials that utilize both UV and visible light can be engineered. Bekele and Alamnie (2025) mention that various semiconductor metal oxide NPs like ZrO_2, ZnO, V_2O_5, TiO_2, Fe_2O_3, WO_3, CeO_2, Cu_2O, CdS, ZnS have been used as photocatalysts in various studies for applications including water remediation and further note that development of metal/metal, metal/metal oxide and metal/carbon composite heterojunctions has greatly enhanced photocatalytic capabilities as compared to the single-phase photocatalysts. Single phase photocatalysts such as ZnO, CuO, etc encounter a grave problem of quick electron-hole recombination which can

be eliminated through development of heterojunction so that these charges get efficiently separated. Zhang et al. (2026) observe that BDC based photocatalytic composite material show superior photocatalytic performance because carbon matrix acts as a good electron acceptor and hence prevents charge recombination during photocatalysis. Also, carbon matrix provides good scaffold for the photocatalytic agent. Furthermore, it helps to bind the pollutants onto itself so that ROS produced by the photocatalytic sites can quickly degrade the pollutant. According to them, bottom -up synthesis method of BDC based composites uses hydro-soluble carbohydrates to synthesize photocatalyst composites by HTC method. In the top-down synthesis method, naturally available biomass precursors are utilized. Due to their cost-effectiveness and ease of synthesis, the top-down approach of BDC composites is more convenient.

Since ZnO is a good photocatalyst and it is easy to synthesize on carbon precursor, ZnO/ carbon composites have been widely prepared by various methods and studied for dye degradation as well as water remediation. ZnO/AC composites are the easiest to synthesize via chemical activation of biomass precursor by $ZnCl_2$ or other means and they have shown good adsorptive and photocatalytic properties. Cheng et al. (2016) used Crofton weed to synthesize AC by KOH activation and microwave assisted pyrolysis and recorded monolayer adsorption capacity of 387.6 mg/g for MB dye. Andriantsiferana et al. (2014) used commercial AC produced from coconut and TiO_2 crystals to synthesize TiO_2/AC composite by coating the AC with TiO_2 and achieved 96 % removal efficiency in 3 h for first cycle and 80 %removal efficiency in second cycle. Kumari (2022) used AC prepared from Indian Jujube seeds by chemical activation using $ZnCl_2$ to fabricate ZnO/AC composite by one step facile HTC process. They found hexagonal nanorods of ZnO dispersed on the surface of the AC. The composite successfully degraded MB with 97.25 % removal efficiency in 2 h under UV light. Zhang et al. (2010) used the spent catalyst obtained from vinyl acetate manufacture, carbonized it in N_2 atmosphere at different temperatures of 300 ˚C, 400˚C, 500˚C, 600˚C, 700˚C, 800˚C and 900˚and found that as carbonization temperature increases, the resulting AC composite developed higher porosity. Higher temperature allowed better dispersal of ZnO on the surface. They also observed that ZnO reduced to Zn in the presence of carbon at high temperature and then vaporization of Zn occured as its boiling point is 907˚C. Salah et al. (2024) synthesized firstly AC and then ZnO/AC from olive stones using phosphoric acid activation and studied the capacity of the

composite to adsorb and photodegrade phenol and formic acid. The ZnO/AC composite showed 100% adsorption for phenol within 2 h and lesser adsorption for formic acid. Reusability of the composite after three cycles still remained 97 %. Despite these promising studies, Andriantsiferana et al. (2014) observes that AC composites suffer from some grave problems where carbon/metal oxide ratio becoming too high or too less can reduce photocatalytic activity by blocking light or by blocking pores. Moreover, metal oxide is not strongly bonded to carbon matrix which can cause leaching of metal ions into water. Also, metal oxide particles tend to agglomerate during carbonization process in ZnO/AC composites.

Similarly ZnO/C nanocomposites have been synthesized by other means too and have been studied for photocatalytic degradation. Ngullie et al. (2022) synthesized a novel photocatalyst using pomelo orange biomass waste to create magnetic ZnO supported carbon aerogel (CA) for dye degradation. The ZnO/MNC (75%) showed highest photocatalytic activity in visible light with degradation efficiency of 97.14%. Here, magnetic properties allowed easy recovery and reuse. Maddu et al. (2021) synthesized carbon dots from coffee grounds.Pure ZnO nanoparticles were also synthesized separately. The as synthesized ZnO/CD nanocomposite prepared by one-step one pot method using ultrasonic bath achieved upto 80% of MB degradation under UV light in 150 minutes which was three times more than for pure ZnO. Akir et al. (2017) first synthesized ZnO NP by co-precipitation method and the C-ZnO nanocomposite was then prepared via facile hydrothermal reaction of glucose and ZnO nano particles at 120˚C for 12 h. At concentration of 0.5 gL^{-1}, and Rhodhamine B (RhB) aqueous solution of concentration 5×10^{-6} $molL^{-1}$, 97% degradation was achieved within 120 minutes under visible light. Using scavengers, they determined that $\cdot O_2^-$ and e^- were the main ROS which showed photosensitized degradation of RhB occurred rather than photocatalytic degradation. Bakri et al. (2026) synthesized ZnO/C nanocomposites by microwave assisted precipitation method using starch solution and zinc acetate dihydrate in NaOH (2M) solution. Highest degradation was 92% for ZnO/C 400˚C under UV which followed pseudo first order reaction kinetics was observed. Higher efficiency of nearly 100 % was observed for visible light in 70 minutes indicating enhanced light harvesting capacity of the composite. Wang et al. (2019) used TiO_2 synthesized by sol-gel method and GO prepared from natural graphite powder using modified Hummer's method to synthesize TiO_2/GO composite using HTC at 403K for 12 h. TiO_2/GO (20%) sample showed maximum efficiency of 97.5 % for MB

degradation under visible light at 35 minutes adsorption and 140 minutes degradation. Also, pseudo second order reaction was obtained showing chemisorption occurred in the composite due to π-π overlapping between the GO and MB. Ilhami et al. (2024) pyrolyzed peanut shells and using hydrothermal method synthesized ZnO/carbon composite that displayed star-shaped stacked layers by layer morphology where ZnO was encapsulated between the layers. The composite was found to inhibit bacterial growth effectively under visible light illumination. These studies showed that various nanocomposites of ZnO/C also show excellent photocatalytic properties. ZnO/C nanocomposite using GO sheets shows very good adsorptive capacity as well due to chemisorption by π-π stacking. However, serious limitations of agglomeration due to hydrophobicity and problem of leaching and catalyst recovery exist for these nano composites. As their size is of nanoscale, they can easily escape into the treated water from the various membranes that are supposed to hold them back.

Thus, to overcome the limitations of ZnO/AC composites as well as that of ZnO/C nanocomposites, new approaches have been devised, among which the use of MOF as template for carbonization is one. Though MOFs are mostly studied for carbon capture and energy storage applications, Shahzadi et al. (2024) reviewed the studies on MOF-derived carbon composites and found that along with electrocatalytic degradation of pollutants, it has been studies for photocatalytic degradation also though the volume of such studies is low. Hussain et al. (2018) synthesized MOF 5 and derived ZnO/C nanocomposites by carbonizing it in different conditions at 800˚C and 1000˚C in argon atmosphere. They found that ZnO and Zn disappeared from the samples heated at 1000˚C because Zn vaporizes at around 907˚C. The 1000˚C samples chiefly contained carbon only (96 %). While the 1000˚C samples showed higher adsorption but lower photocatalytic degradation of MB under visible light, 800˚C samples exhibited just opposite behaviour confirming that ZnO was necessary for the photocatalytic degradation. Hussain et al. (2019) again synthesized MOF 5, MOF 74 and ZIF-8 and derived ZnO/C nanocomposites from them. Photocatalytic degradation of MB and H_2 evolution was studied under visible where ZnO/C MOF 5 adsorbed and photodegraded the maximum i.e. 91% MB while ZnO/C MoF 74 and ZnO/C ZIF 8 showed only 65 % and 70 % removal of MB due to smaller pore structures in them through which diffusion of MB molecules was hindered. Cui et al. (2021) observed that MOF-derived carbon composites too suffer from metal particle agglomeration at higher carbonization temperatures because the

carbon matrix may collapse due to rapid shrinkage. We should further note that scalability and high cost are the problems faced by MOF-derived composites as well. Existence of micropores only in MOFs is also a problem in the scenario of pollutant degradations, because pollutants are typically complex organic molecules of large size that cannot diffuse into these micropores of the MOF structures. In this context, incorporation of MOFs with biomass which is seen to promote dispersion of metal active sites homogeneously in the carbon matrix, introduces mesopores and macropores for diffusion and adsorption of pollutants, reduces cost and makes synthesis scalable, can be an effective strategy. Chen et al. (2025) successfully fabricated novel N-doped Zr/carbon composite by growing Zr-MOFs in situ on bagasse followed by its pyrolysis. They used this composite as anode in electrocatalytic application for effective removal of phosphorus from water as Zr is highly selective towards phosphorous. Similarly, Zhao et al. (2020) synthesized carbon aerogels having hierarchical porous network by in situ growth of an MOF, MIL-53 on kapok fibers followed by its direct carbonization. This aerogel exhibited superb water repellant property and showed high adsorptive capacity towards oils and organic solvents. Gao et al. (2022) grew ZIF-8 on cornstalk/ cornstalk biochar and pyrolyzed them to obtain MOF based carbon matrix composite that they studied for electrochemical energy storage.

From the above discussions, we see that MOFs- biomass derived carbon composites are viable but underexplored alternatives for photocatalytic degradation of pollutants. Though some studies have been done in synthesis of carbon composites directly from MOFs and their photocatalytic performance has been studied, almost no study has been done on photocatalytic degradation of pollutants from MOFs- biomass derived carbon composites. Since ZIF-8 MOF can be synthesized by facile means in aqueous medium as well, we therefore attempt to synthesize ZIF-8 on a biomass substrate in water medium to derive ZNO/C composite from it upon direct carbonization. Though any biomass substrate can be used, it should be noted that the biomass source must be sustainable, easy to grow, cheap, having valorisation potential, with properties that can enhance the performance of the carbon composite and novel. In this context, *Azolla pinnata* biomass easily comes to our mind. It is a very fast-growing aquatic fern even studied for its phytoremediation properties in water remediation. It can turn invasive in some environments. It can uptake toxic heavy metals to some extent and can be grown in wastewater itself (Akinbile et al., 2016) Moreover, this biomass is also an underexplored

source of nanoporous carbon though it has lignocellulosic structure that yields hierarchical porous carbon and has high nitrogen content that is beneficial for N-doping of carbon matrix turning it sensitive to visible light. Hence, we found a research gap in the literature on synthesis of metal oxide/ carbon composites by in situ growth of MOF on *Azolla pinnata* biomass surface. So, this work will be novel. Further, we are attempting to grow ZIF-8 in aqueous medium instead of an organic solvent, thereby making the synthesis process green and more cost- effective as water medium will offset the cost of expensive ZIF-8 precursor, 2-methyl imidazole. Studies to evaluate the photocatalytic degradation capacity of such MOF based biomass derived composites have not been conducted so far, to our knowledge.

CHAPTER 3: MATERIALS AND METHODS

3.1 Research Methodology

We attempt to synthesize ZIF-8 incorporated *Azolla pinnata* biomass, then carbonize it in inert atmosphere at different temperatures, characterize it using various characterization techniques and then used the as synthesized ZnO/C composite to degrade MB dye in an aqueous solution and hence evaluate its performance and perform kinetic studies.

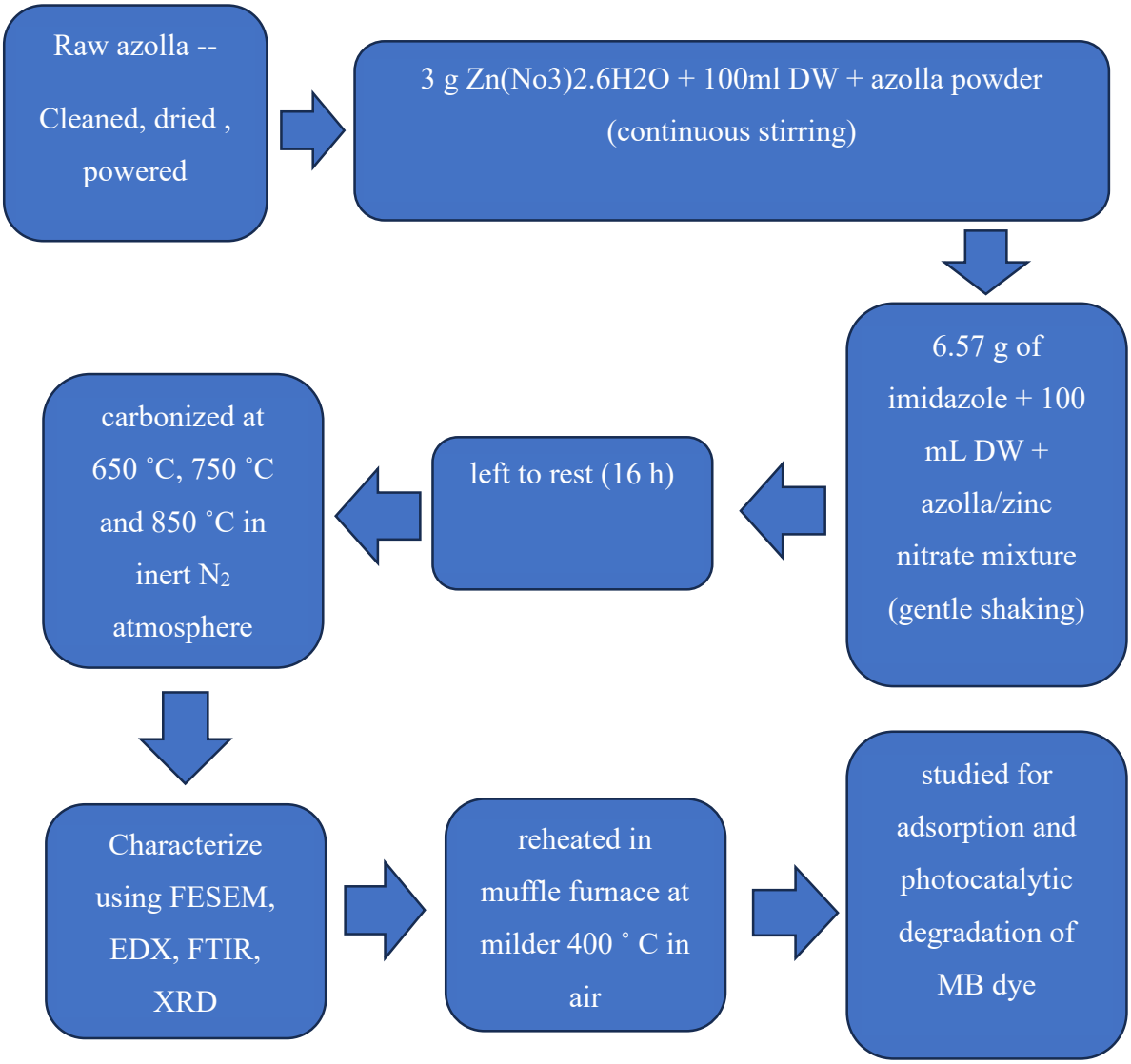

3.2 Materials Used

Raw Azolla pinnata biomass, distilled water (DW), zinc nitrate hexahydrate, 2-methylimidazole (Hmim) as the organic linker, methylene blue (MB) dye.

All reagents used in this study were analytical grade. Raw Azolla pinnata biomass was obtained from a nearby farm located in Kathmandu valley.

A 250 ml solution of MB of 10 ppm concentration was prepared by mixing 2.5 g of MB in 250 mL distilled water as stock solution of MB.

3.3 Instruments and Apparatus

The various instruments and apparatus that were used during the entire course of study are listed below:

a) Hotbox Oven (Gallenkamp Registered Trade Mark Hotbox Oven)

b) Tubular furnace (Kejia)

c) Muffle furnace (Scarlett Alloys Wire, Kolkata)

d) Magnetic Stirrer

e) UV source (OmniCure Series 1500, Shimadzu Corp.)

f) Curing Chamber (Figure 6(d))

g) UV- vis spectrometer (UV-2600i, Shimadzu Corp.)

h) Centrifuge Rotator (Centrifuge 80-2)

i) FTIR (PerkinElmer Spectrum IR Version 10.6.2)

j) FeSEM/EDX (JEOL JSM)

k) XRD

FTIR was carried out in Amrit Science College (ASCOL), Lainchaur, Kathmandu, Nepal

FeSEM/EDX and XRD were done in Jeonbuk National University, South Korea

3.4 Preparation of azolla derived ZnO-carbon composite

The raw *Azolla pinnata* biomass (APB) was washed, cleaned and sundried for a day, kept in the oven for 18 hours at 80˚C to dry. The dried APB was then ground to powdered form and sieved through 212micron sieve. Then, 3 g zinc nitrate hexahydrate $Zn(NO_3)_2.6H_2O$ was dissolved in 100 mL DW in which 5 g of APB powder was mixed with continuous magnetic stirring for 3 hours. After that, 6.57 g of imidazole was dissolved in 100 mL of DW and gradually added to the APB-zinc nitrate solution with gentle shaking. Then it was kept to rest for 16 hours at room temperature to allow the growth of ZIF-8 MOF on APB surface. This surface-modified sample was then drained of the solvent, allowed to dry in the oven, and then carbonized in an inert atmosphere at three temperatures – 650˚C, 750˚C and 850˚C (± 20 ℃) in a tubular furnace. The carbonized samples were named ZnO/C650, ZnO/C750 and ZnO/C850, respectively. The APB powder prior to growth of MOF on it was regarded as the pristine sample.

3.5 Characterization

The surface morphology and elemental composition of the pristine azolla powder and carbonized samples ZnO/C650, ZnO/C750 and ZnO/C850 were studied by FeSEM/EDX. Similarly, presence/absence of various functional groups and confirmation of formation of ZnO nanoparticle was studied using FTIR spectroscopy. XRD was used to analyze the formation and size of ZnO NPs anchored on the carbon matrix. Finally, the performance of the ZnO/C composites carbonized at various temperatures in degradation of MB dye from an aqueous solution was studied using UV-vis spectroscopy.

3.5.1 Photocatalytic degradation of MB dye from aqueous solution

The carbonized samples ZnO/C650, ZnO/C750 and ZnO/C850 were again reheated at a mild 400˚C for half an hour in a muffle furnace. This step helps to refine the carbonized sample surfaces by converting any ZnO reduced to Zn by carbon back to ZnO. It improves contact between carbon and ZnO particles and increases the crystallinity of ZnO (Hu et al., 2020). MB solutions of 10 ppm concentration in neutral conditions (pH 7) were prepared from the stock solution and 10 mg of each sample, ZnO/C650, ZnO/C750 and ZnO/C850 were loaded into 50 ml MB solution (**Figure 7** (a)), stirred for 30 minutes in the dark till they reached adsorption

equilibrium (Akir et al., 2017). The stirring was then continued for time intervals of 15, 45, 60, 90, and 120 minutes (**Figure 7**(b)), respectively, under UV light from a UV source (**Figure 7**(d)).

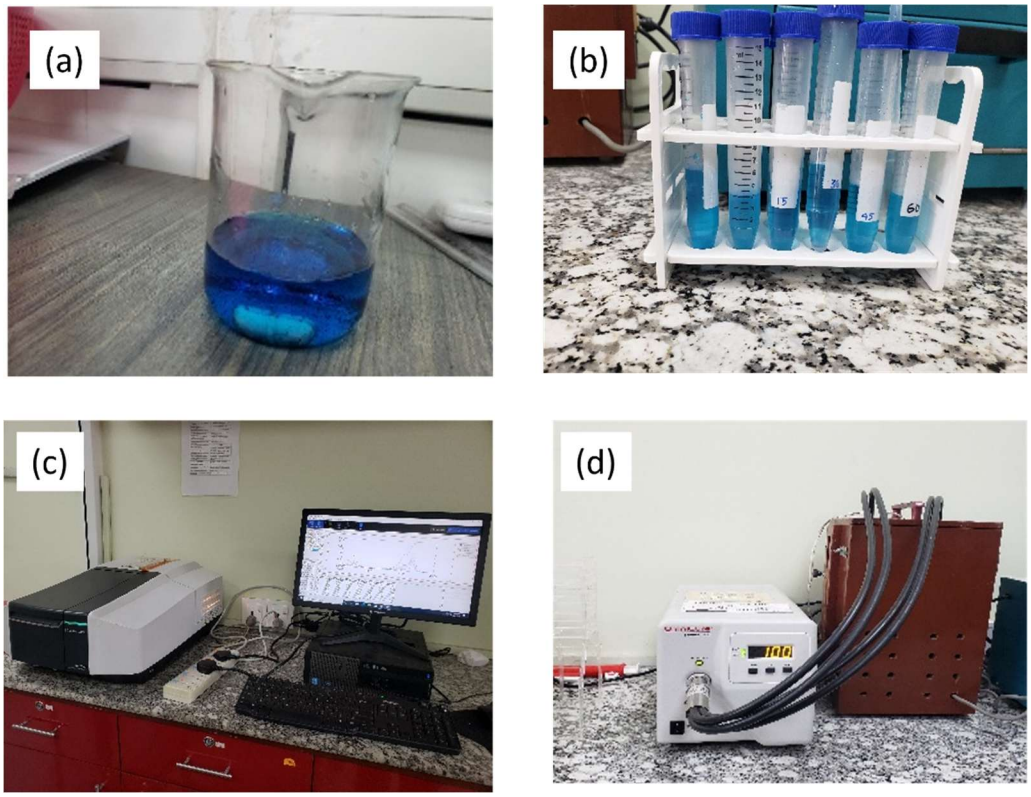

Figure 7: a) 10 mg ZnO/C650 loaded in 50 mL MB solution (b) MB solution samples loaded with ZnO/C650 at different time intervals (c) UV vis spectrometer (d) UV source and curing chamber

Solution samples were collected after each time interval and the removal efficiency was studied using UV-vis spectrophotometer (**Figure 7**(c)). The MB dye has an absorbance peak at 664 nm followed by a shoulder at 620-610 nm in the visible region. These peaks can be used to obtain the maximum absorbance of visible light by MB dye solution and using Beer-Lambert law , concentration of MB dye in the solution can be calculated by plotting the calibration curve of maximum absorbance vs. known concentration.

According to Beer-Lambert's law, the peak absorbance by MB dye solution and concentration of MB in the solution are directly proportional to each other as given by,

$$\frac{C_t}{C_0} \approx \frac{A_t}{A_0} \qquad (1)$$

where A_0 = the initial max. absorbance by the blank MB solution

C_0 = the initial concentration of the blank MB solution

A_t = the max. absorbance by the loaded MB solution at some time interval, *t* and

C_t = the concentration of the loaded MB solution at some time interval, t

And the relation between absorbance A and concentration C holds as

$$C = \frac{A}{\varepsilon} \qquad (2)$$

Here, C is in $molL^{-1}$ and ε is the molar absorptivity of MB which is approximately 95000 $mol^{-1}cm^{-1}$ for 664 nm and the typical cuvette width is 1 cm.

The degradation rate or removal efficiency can be calculated as

$$Degadation\ \% = \frac{C_0 - C_t}{C_0} \times 100\% \qquad (3)$$

3.5.2 Study of reaction kinetics of adsorption and photodegradation of MB dye

The reaction kinetics can be studied for pseudo-first order kinetic using Langmuir-Hinshelwood model given by the equation

$$\ln\left(\frac{C}{C_0}\right) = -kt \qquad (4) \qquad \text{(Kumari, 2022)}$$

In which C = concentration of dye after time t (mg/L)

C0 = initial concentration of dye (mg/L)

k = rate constant that can be evaluated from the plot of – ln (C/C0) vs. time

t = time

The pseudo-second order kinetics can be expressed in the form given by

$$\frac{t}{q_t} = \frac{1}{k_2 q_e^2} + \frac{t}{q_e} \qquad (5) \qquad \text{(Zhang et al., 2013)}$$

where q_t = amount of MB dye degraded at time, t (mg/g)

q_e = equilibrium capacity given by the plateau value of concentration (mg/g)

t = time

k_2 = rate constant for pseudo second order reaction.

q_t is obtained using the relation,

$$q_t = \frac{(C_0 - C_t) \times V}{m} \qquad (6)$$

and experimental q_e is obtained using the relation,

$$q_e = \frac{(C_0 - C_e) \times V}{m} \qquad (7)$$

in which t = time

C_t = concentration of MB at time, t

C_0 = initial concentration of MB

C_e = equilibrium concentration of MB

m = loading mass of ZnO/C composite (g)

V = volume of MB dye solution (L)

The plot of t/q_t vs. t will be used to obtain the rate constant and calculated q_e. For pseudo second order reaction kinetics to be followed, fitted R^2 values must be close to one and the experimental q_e and calculated q_e must be close to each other (Zghal et al., 2023).

3.5.3 X-ray diffraction (XRD)

Using the XRD peaks obtained for ZnO NPs embedded in the carbon matrix of ZnO/C samples, we can obtain the average particle size of the ZnO particles using the relation

$$D = \frac{K\lambda}{\beta cos\theta} \qquad (7)$$

where D = size of the particle,

K = Scherer's constant taken as K = 0.95 for spherical particles

λ = wavelength of X-ray (for Cu $K\alpha_1$, λ = 1.5406 Å)

β = full width at half maximum (FWHM) of the diffraction peak

θ = half of any 2θ peak obtained in the XRD pattern.

3.5.4 FTIR Spectroscopy

Fourier Transform Infrared Spectroscopy (FTIR) is a non-destructive analytical technique used to characterize chemical composition and presence of functional groups in the sample molecules and also to identify then. It uses Michelson interferometer to scan the sample across the infrared (IR) spectrum and records the transmittance or absorbance of each specific IR wavelength. In FTIR spectrum, the region above 1500 cm^{-1} is used to analyze functional groups present in the sample and the region below 1500 cm^{-1} is called the fingerprint region which is useful if we already know what molecules we expect to find.

3.5.5 FeSEM/EDX Analysis

Field Emission Scanning Electron Microscope (FeSEM) is used to obtain the surface features and morphology of micro and nanoscale particles. An electron gun shoots a sharp electron beam onto the sample. Depending upon the surface structure these electrons are either absorbed or reflected. A detector then analyses the intensity of scattered electron beam to determine the surface properties. SEM is often accompanied by Elemental Dispersive X-ray (EDX) analysis capabilities in which the secondary augur electrons that have been knocked off the sample are detected and analysed to obtain its elemental composition.

CHAPTER 4. RESULTS AND DISCUSSIONS

Biomass derived ZnO/carbon composite was synthesized by growing ZIF-8 MOF on Azolla pinnata biomass substrate in aqueous medium followed by its carbonization under inert N_2 atmosphere in various temperatures of 650˚C, 750˚C and 850˚C. The as prepared ZnO/C composite samples were named ZnO/C650, ZnO/C750 and ZnO/C850 respectively. The surface textural properties, morphology and elemental of the pristine azolla biomass, ZIF-8 incorporated azolla biomass and the three carbonized samples was studied using FeSEM and their elemental compositions were mapped by EDX. Further, FTIR analysis was done on the pristine and carbonized samples to verify the formation of ZnO/C carbon composites. Also, XRD analysis was done to study the nature of ZnO particles embedded in the carbon matrix as well as to ascertain the phase of carbon matrix itself. Then, adsorption and photocatalytic degradation capacity of the as -prepared samples was studied for degradation of MB dye by first stirring the MB dye solution loaded with the different samples in dark for 30 minutes followed by UV exposure for another 120 minutes. Samples of this solution at different time intervals of 30 minutes in dark followed by 15, 30, 45, 60, 90 and 120 minutes under UV exposure are taken and their UV- vis absorbance was measured using UV- vis spectrometer. The maximum absorbance values obtained at 664 nm for each sample was then used to find the concentration of MB dye in the aqueous solution at different time intervals. The change in concentration of MB dye in the aqueous solution with time was then studied and degradation efficiency of each sample was ascertained. Similarly, the as obtained concentration data were fitted for pseudo first order and pseudo second order reaction kinetics to find how the adsorption and degradation of MB dye proceeded under the action of ZnO photocatalyst.

4.1 Characterization of ZnO/carbon composites

4.1.1 FeSEM image and EDX analysis

FeSEM image of the pristine azolla sample shows smooth surface texture of the biomass substrate (**Error! Reference source not found.**(a)). FeSEM image of the zinc -incorporated

azolla substrate (**Error! Reference source not found.**(c)) shows elongated and flattened hexagonal flaky crystallite structures growing on the surface of the biomass. This confirms the formation of ZIF-8 MOF structures on the biomass substrate. (**Error! Reference source not found.**(b)) shows that ZIF-8 crystals have grown evenly all over the biomass substrate. The even growth of the ZIF -8 crystals will help to increase the surface area of the substrate upon carbonization. The crystallites were observed to be distributed evenly on the surface of the biomass.

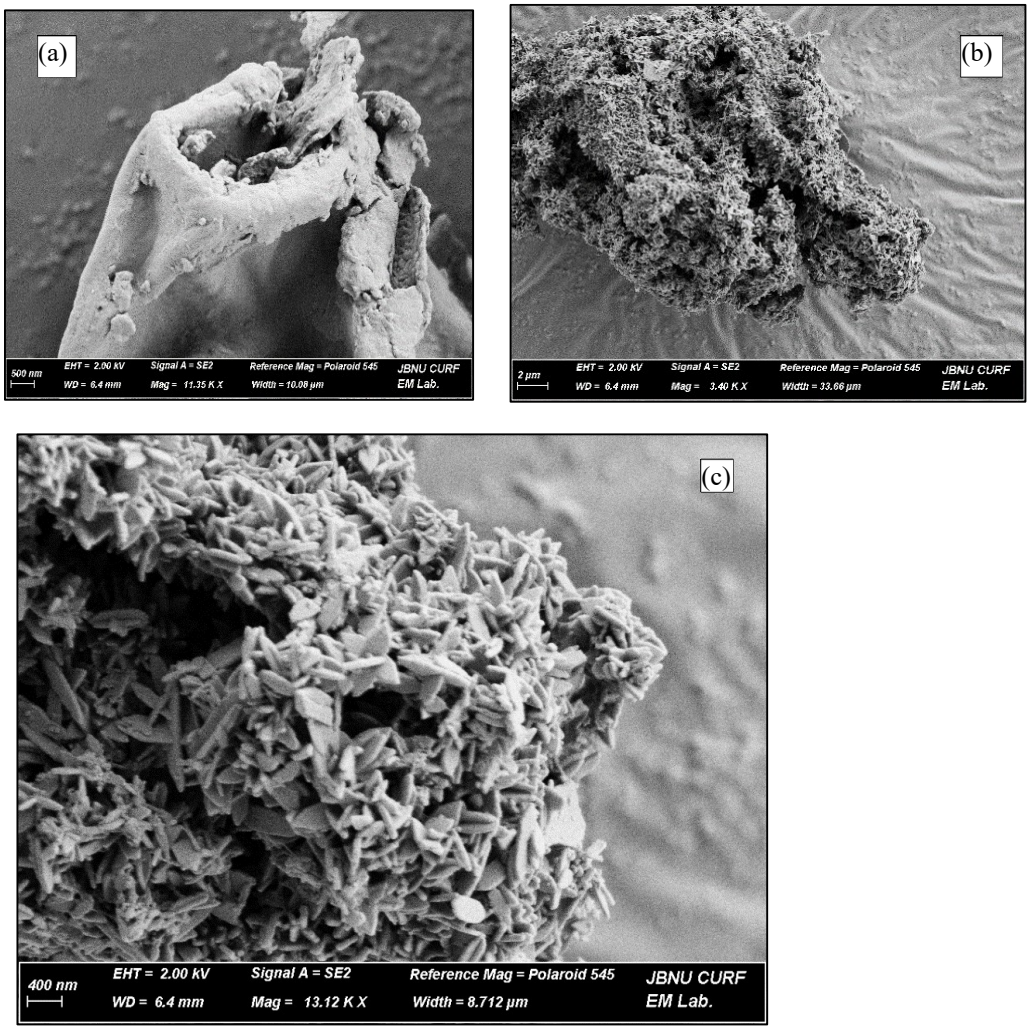

Figure 8: (a) *Azolla pinnata* pristine biomass substrate (b) ZIF-8 crystallites seen growing homogeneously on the azolla substrate (c) closer view of (b), flattened and elongated flaky crystallites of ZIF-8

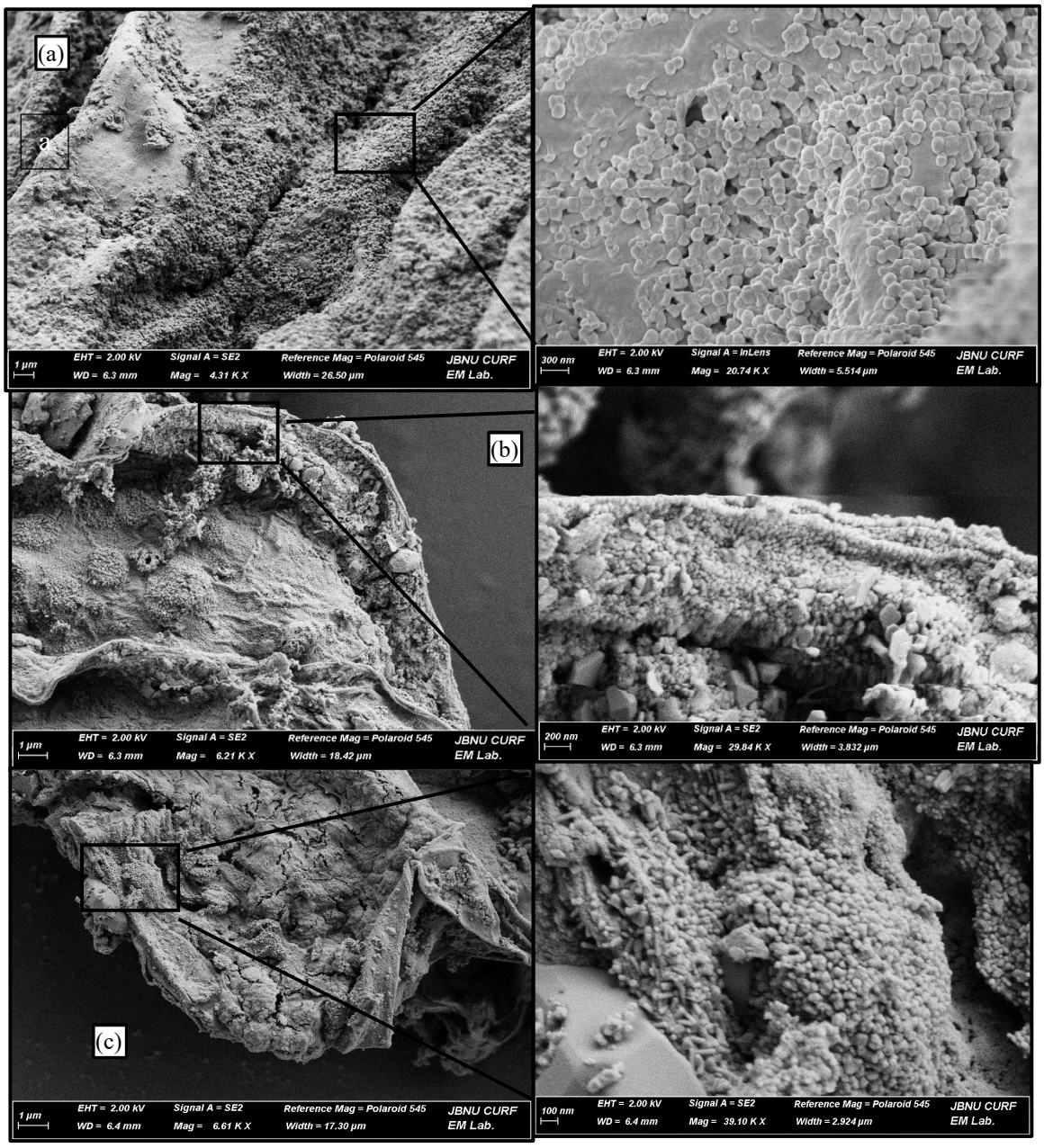

Figure 9: (a) ZnO/C650 composite surface (b) ZnO/C750 composite surface (c) ZnO/C850 composite surface

On carbonization under inert conditions, FeSEM image for ZnO/C650 sample (**Figure *9***(a)) shows some change in morphology where the crystallite structure of ZIF-8 is destroyed and the size also reduced due to vaporization of water and other organic volatiles forming well dispersed bead like structure on the surface of the substrate. FeSEM image of ZnO/C750

sample (**Figure *9***(b)) shows the bead like structures formed due to carbonization of the ZIF-8 on azolla substrate further shrinks in size almost by half than that of ZnO/C650. ZnO/C850 sample follows this trend and has the smallest bead like structures uniformly distributed on carbonized azolla biomass substrate (**Figure *9***(c)).

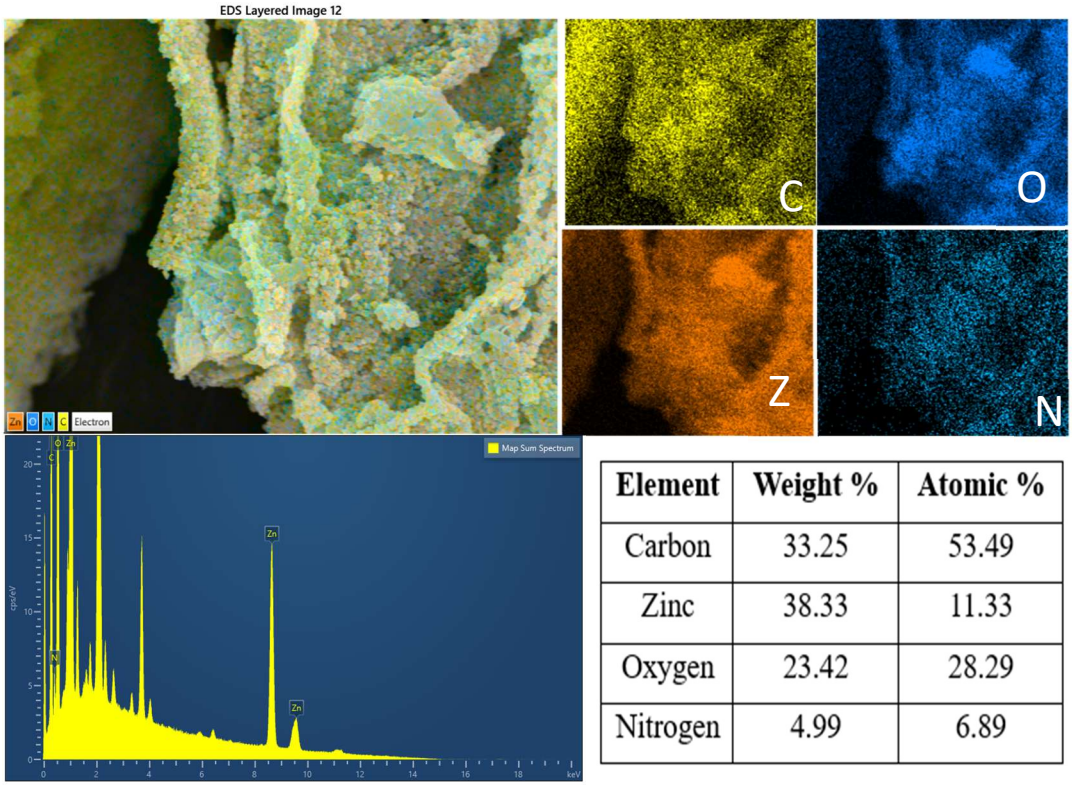

Element	Weight %	Atomic %
Carbon	33.25	53.49
Zinc	38.33	11.33
Oxygen	23.42	28.29
Nitrogen	4.99	6.89

Figure 10 Elemental Composition of ZnO/C850 sample obtained from EDX

EDX analysis of the carbonized ZnO/C850 sample shows the presence of carbon, oxygen, zinc, and a trace amount of nitrogen. The weight % and atomic % of the elements present in the sample ZnO/C850 as obtained through EDX analysis is presented in **Figure *10*Error! Reference source not found.**. Zinc atoms were seen to be evenly dispersed throughout the sample with a significant presence of oxygen as well. This indicated oxygen-rich functional groups on the surface. Trace amount of 6.89 % of nitrogen confirmed N-doping of the carbon matrix due to nitrogen rich content of azolla biomass.

In **Figure *10***, we see that the Atomic % of carbon is 53.49 % while that of zinc in zinc oxide is 11.33%. Oxygen atomic % is found as 28.29 % indicating presence of O-containing functional groups on the surface. Trace amount of N is also seen indicating N- doping which was obviously incorporated into the carbon matrix from both the imidazole linkers of ZIF-8 crystals and the N-rich azolla biomass.

4.1.2 FTIR analysis of pristine azolla and ZnO/C composites

The FTIR spectra obtained for the pristine azolla and the three carbonized samples ZnO/C650, ZnO/C750 and ZnO/|C850 are presented in **Figure 11**.

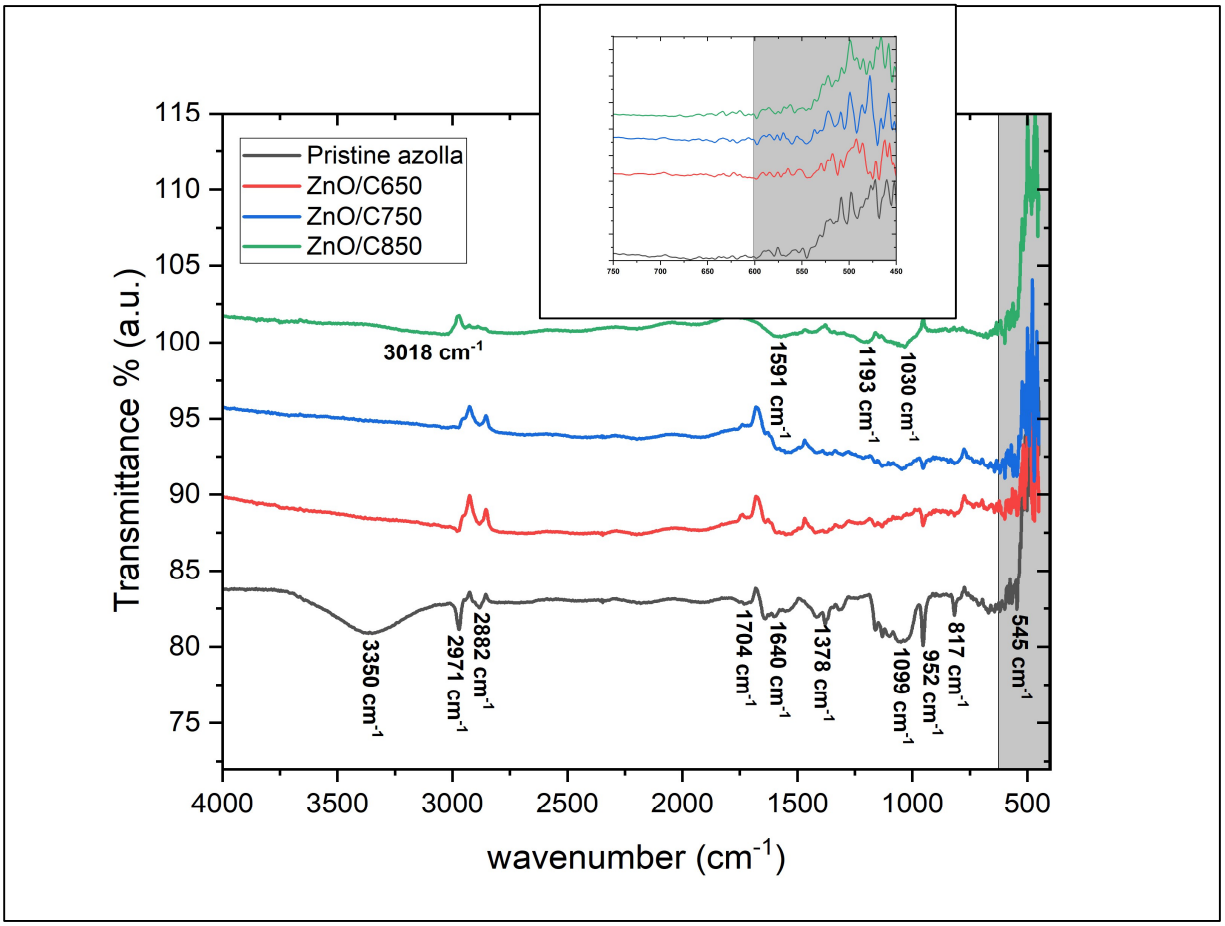

Figure 11: FTIR spectra obtained for the pristine azolla and the three carbonized samples ZnO/C650, ZnO/C750 and ZnO/C850

FTIR characterization was done for the confirmation of carbonization of the Zn-incorporated azolla biomass and also for the indication of ZnO in the carbon composite sample. The FTIR spectrum of pristine azolla (presented in black) is indictive a lignocellulosic biomass with high protein content. A strong broad band is seen at 3350 cm^{-1} which indicates O-H stretching vibration of water trapped inside the biomass matrix. There is also contribution from N-H (amine) group in this region. Two peaks at 2971 cm-^{1} and 2882 cm^{-1} are due to aliphatic stretching vibrations of CH_2/CH_3 in biomass matrix signaling presence of hydrocarbons, lipid or wax. A small broad band 1704 cm^{-1} represents C = O stretching vibrations of carbonyl group related to hemicellulose, pectin and lipids. 1640 cm^{-1} to 1537 cm^{-1} small peaks signify an overlap of C = O stretching of peptide bonds in protein, N - H bending and C - H vibrations from protein secondary structures and also C = C stretching from lignin. The 1378 cm^{-1} peak is a hallmark of cellulose and hemicellulose and its sharpness indicates higher crystallinity of cellulose. Smaller 1307 cm^{-1} peak indicates C - O stretching or C – H bending from lignin or hemicellulose. The 1163 cm^{-1} to 1022 cm^{-1} region is the carbohydrate fingerprint region where there is some overlap and hence broadening due to silicate groups that may bio-accumulate in azolla biomass. 952 cm^{-1} sharp high intensity peak is due to glycosidic linkage vibrations in cellulose/hemicellulose. However, this can also indicate Si – OH bending due to SiO_2 accumulation. A sharp 545 cm^{-1} peak indicates presence of inorganic mineral constituents i.e. metal-oxygen linkages in pristine azolla.

It is observed that, upon carbonization peaks due to various functional groups begin to disappear or become smaller. This trend increases and the spectrum smooths out as carbonization temperature increases because at high temperature most of the organic volatiles and water formed from the functional groups and hydrogen vapourize. In ZnO/C650 and ZnO/C750 spectra, it is observed that the C = O bond persists showing presence of -COO functional group in the ZnO/C matrix. In ZnO/C850 however, broad bands appear at 3018 cm^{-1}, 1591 cm^{-1}, 1193 $cm^{-1}$and 1030 cm^{-1}. 3018 cm^{-1} broad peak is indicative of sp^2 C-H stretching of aromatic C-H groups or of H trapped in disordered char like environment of the carbon matrix. 1193 cm^{-1} indicates C=N stretching which means the carbon matrix had become N-doped and and C=C as well that shows presence of aromatic small disordered pockets of turbostratic carbon rather than ordered graphitic planes. 1193 cm^{-1} represents C-N or C-O. But at 850 ˚C in ZnO/C composite this peak strongly represents C – O – Z linkage which signifies

ZnO is not just physically in contact but is chemically bonded to the carbon matrix. At high temperatures, a broad 1030 cm^{-1} also indicate Zn – O – C bonds or C – O bonds trapped between ZnO and carbon substrate.

Furthermore, extra peaks appear in all three ZnO/C composites at 400-600 cm^{-1} (**Figure 11** inset) region which are indicative of ZnO nanostructures embedded in the composite. In ZnO/C850, we clearly observe a sharp peak at 598 cm^{-1} that shows strong Zn – C coupling of ZnO and carbon matrix. Thus, the FTIR analysis confirms successful formation of ZnO/C carbon composites with functional groups of O present in ZnO/C650 and ZnO/C750 while emergence of Zn-O-C and Zn-C bonds and turbostratic carbon pockets in ZnO/C850 sample. These findings are in agreement with the temperature dependence of nature of carbon composite.

4.1.3 XRD Analysis

The formation of wurtzite structure of ZnO NPs can be further conformed by X-ray diffraction analysis. Also, the nature of carbon present in the biomass carbon matrix can be identified. The XRD pattern obtained for ZnO/C650, ZnO/C750 and ZnO/C850 samples are shown in **Figure *12***. The main characteristic peaks of ZnO wurtzite hexagonal structure are indexed with Miller indices (hkl) which represent the interplanar spacing and orientation of the planes.

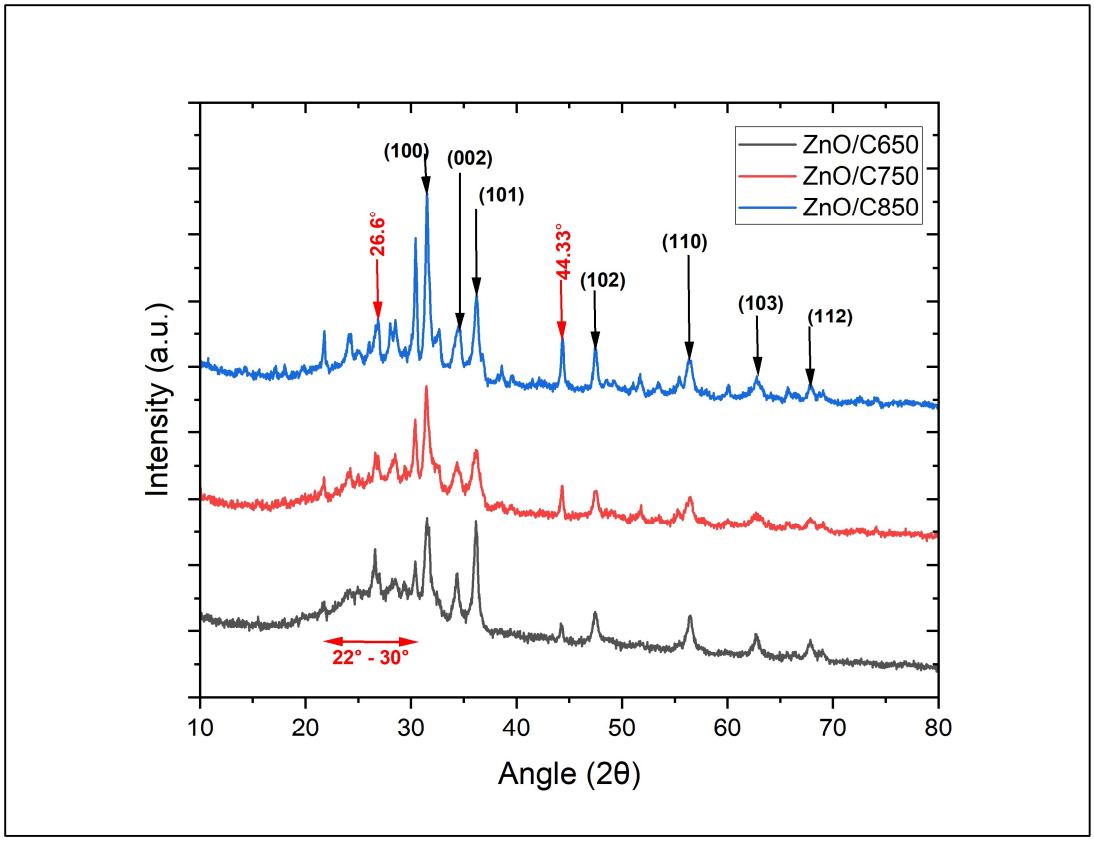

Figure 12: XRD pattern obtained for ZnO/C650, ZnO/C750 and ZnO/C850

The main sharp peaks of ZnO wurtzite structure are observed at 31.5˚, 34.48˚, 36.23˚ corresponding to (100), (002) and (101) planes. Similarly, minor peaks of ZnO wurtzite are seen at 47.43˚, 56.32˚, 62.77˚ and 67.85˚ corresponding to (102), (110), (103) and (112) hkl planes (Maddu et al., 2021). These peaks are seen in all three samples, confirming formation of ZnO crystals in all of them. The peaks are sharper for ZnO/C850 which shows due to higher temperature of carbonization, more crystalline ZnO particles were formed in that sample.

Furthermore, a broad hump of low intensity around 22˚ - 26˚ can be observed more prominently in XRD patten of ZnO/C650 which indicates the amorphous nature of carbon formed at lower carbonization temperatures. This hump decreases in intensity in ZnO/C750 and almost disappears in ZnO/C850 (**Figure *12***). Two sharp peaks at 26.7˚ and 44.3˚ indicative of graphitic carbon are seen to increase in intensity as temperature of carbonization increases. This shows ratio of sp^2 hybridized graphitic carbon formed is higher for higher temperature carbonization.

Other extra peaks are also observed in all three samples at 21.79˚, 24.1˚, 28.3˚, 30.43˚, 38.53˚ and 51.74˚. These peaks are due to formation silica/silicate and calcite compounds related to the mineral and ash content of azolla biomass. These peaks too become sharper with higher temperature indicating better crystallization. Though these silica/silicate and calcite impurities can be removed by acid wash, as they do not affect the photocatalytic capacity of the composite negatively, so they need not be removed.

The particle size of the ZnO NPs formed after carbonization was calculated for all three samples using the Debye-Scherrer equation (7). The average crystallite size was found to be 8.8 nm for ZnO/C650, 7.8 nm for for ZnO/C750 and 13.55 nm for ZnO/C850. At higher temperature, larger crystallite is formed with higher degree of crystallization and in lower temperature ZnO is in more amorphous form.

4.2 Adsorption and photocatalytic performance of ZnO-carbon composites

The adsorption capacity and photocatalytic action of ZnO/C carbon composites were studied systematically by loading 50 mL of 10 ppm aqueous solution of MB with 10 mg of ZnO/C650, ZnO/C750 and ZnO/C850 each and the change in concentration of MB was studied with time via measurement of UV-vis absorbance by the MB dye samples taken in vials from the 50 mL solution at different time intervals.

Figure 13 shows the calibration curve obtained by plotting absorbance of UV-vis by MB dye solution vs the known concentration of MB dye in aqueous solution. Using this curve, we convert absorbance into concentration of MB dye in accordance with Beer-Lambert law as given in Equation (1).

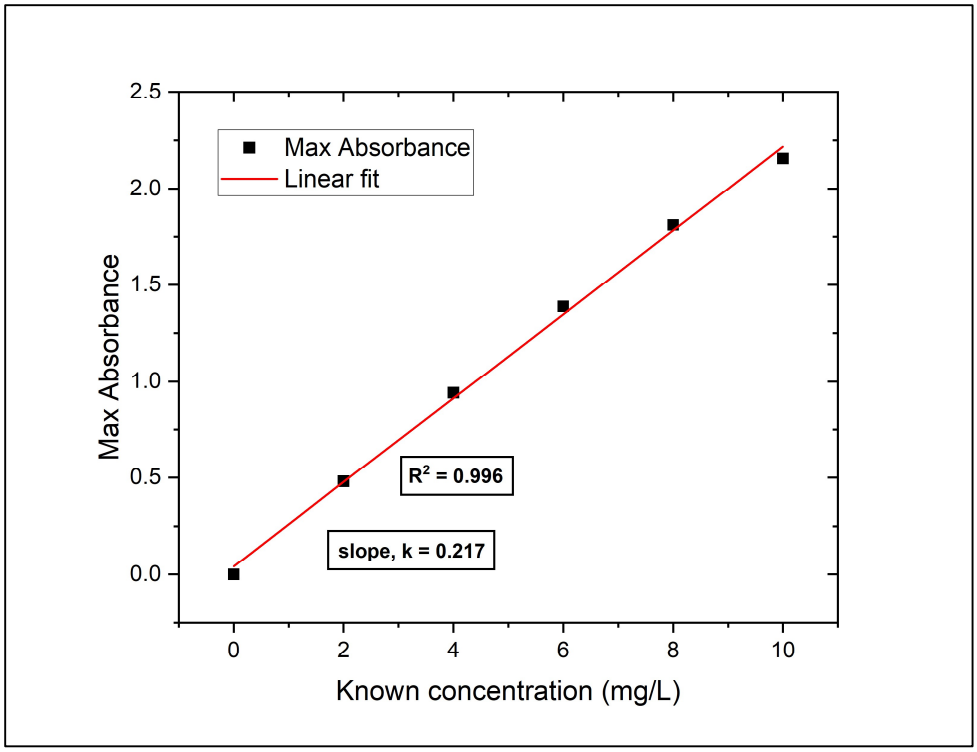

Figure 13: calibration curve obtained by plotting absorbance vs known concentration

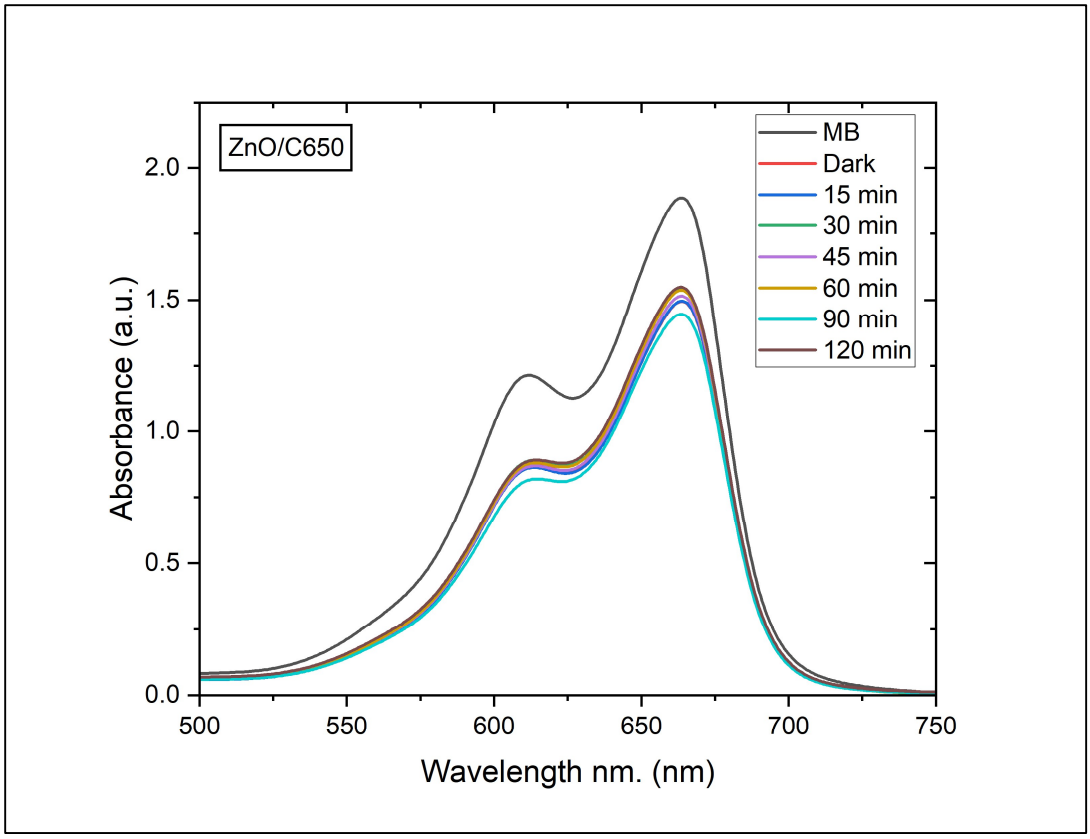

Figure 14: Absorbance of UV-vis by the MB solution samples at ZnO/C650

Table 2 : Degradation efficiency for ZnO/C650

Degradation efficiency for ZnO/C650			
Time (min)	Max absorbance	Concentration (mg/L)	Removal efficiency %
0	1.89	8.69	0.00
30	1.55	7.13	17.92
15	1.54	7.12	18.13
30	1.54	7.08	18.56
45	1.52	6.98	19.67
60	1.50	6.89	20.68
90	1.49	6.88	20.78
120	1.45	6.66	23.33

Absorbance of UV-vis by the MB solution samples loaded with three ZnO-carbon composites samples ZnO/C650, ZnO/C750 and ZnO/C850, respectively, was recorded for different time intervals. MB absorbs light strongly at 664 nm with a shoulder at around 600 nm. Higher absorbance at 664 nm indicates a higher concentration of MB in the solution and vice versa. For ZnO/C650, change in absorbance of UV-vis by MB dye at various intervals of time is shown in **Figure *14***. The corresponding concentration of MB in the sample after each interval is shown in ***Table 2***. It is observed that after the 17% initial reduction in concentration due to adsorption of MB dye by the ZnO/C650 carbon matrix, during UV irradiation for the next 120 minutes there is very nominal change. From the 17.92 % initial removal of the MB dye due to adsorption by carbon matrix to overall 23.33% removal after 120 minutes of UV irradiation shows that photocatalytic activity accounted for only 5.41 % removal. Similar results are seen for change in concentration of MB dye under the action of the ZnO/C750 composite as shown in **Figure *15*** and **Error! Reference source not found.** . While 20.63 % of MB dye was removed from the solution through adsorption by the carbon composite within the initial 30 minutes of stirring in dark, upon stirring under UV light, MB concentration decreased very slowly with most changes seen in the first 15 minutes (3.18%) and at the last 30 minutes (2.64%) of stirring. Total removal efficiency was only 29.10 % even after additional 120 minutes of stirring under UV radiation. This shows that while adsorptive capacity of ZnO/C750 was 20.63%, photocatalytic efficiency was only 8.47 %. There was only a slight increase in both adsorptive capacity as well as photocatalytic activity for ZnO/C750 as compared to ZnO/C650.

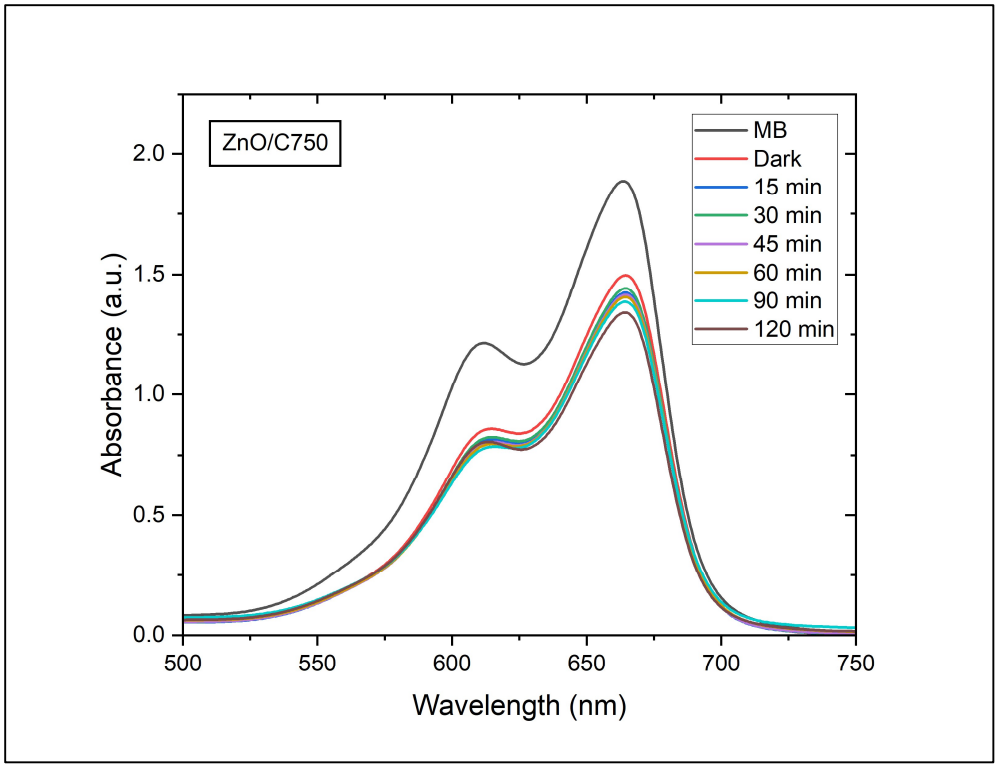

Figure 15: Absorbance of UV-vis by the MB solution samples at ZnO/C750

Table 3: Degradation efficiency for ZnO/C750

Degradation efficiency for ZnO/C750			
Time (min)	Max absorbance	Concentration (mg/L)	Removal efficiency %
0	1.89	8.71	0.00
30	1.50	6.91	20.63
15	1.44	6.64	23.81
30	1.42	6.54	24.87
45	1.42	6.54	24.87
60	1.41	6.50	25.40
90	1.39	6.41	26.46
120	1.34	6.18	29.10

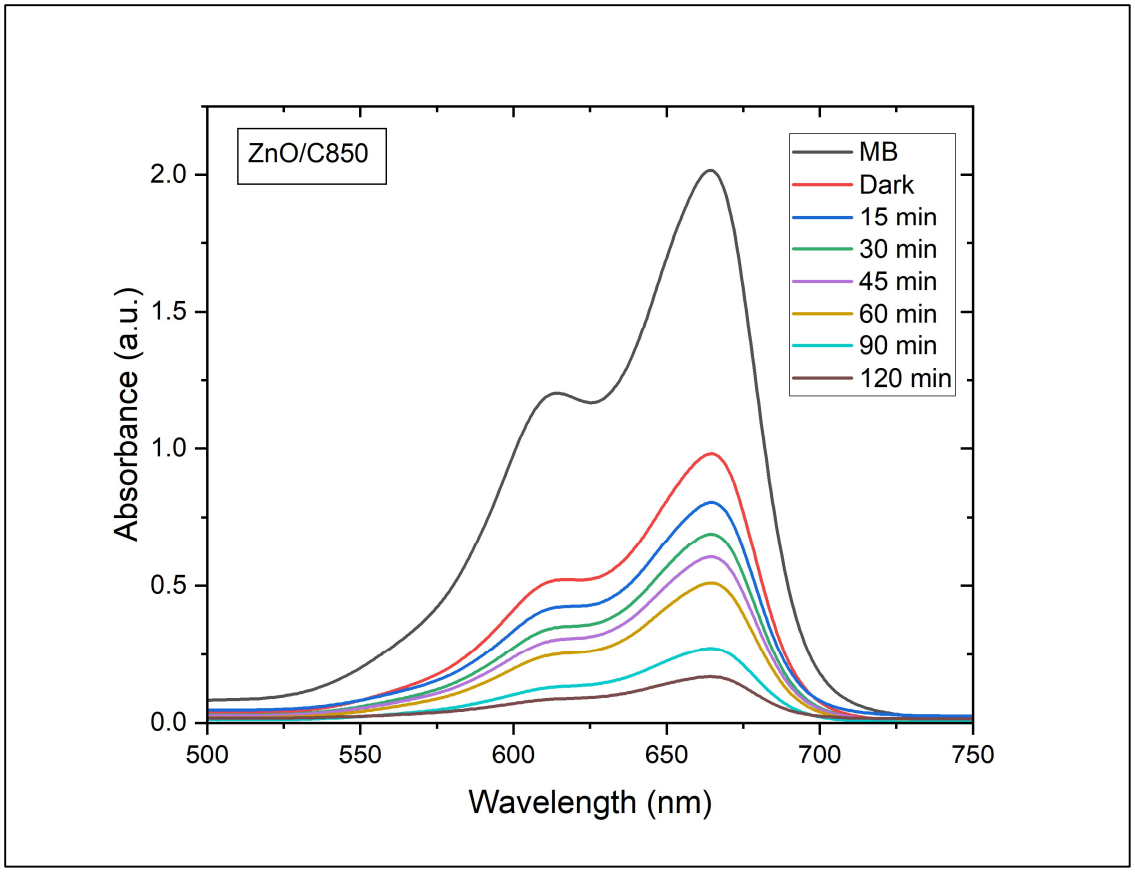

Figure 16: Absorbance of UV-vis by the MB solution samples at ZnO/C850

Table 4: Degradation efficiency for ZnO/C850

Degradation efficiency for ZnO/C850			
Time (min)	Max absorbance	Concentration (mg/L)	Removal efficiency %
0	2.02	9.31	0.00
30	0.98	4.52	51.49
15	0.80	3.69	60.40
30	0.69	3.18	65.84
45	0.60	2.76	70.30
60	0.51	2.35	74.75
90	0.27	1.24	86.63
120	0.17	0.78	91.58

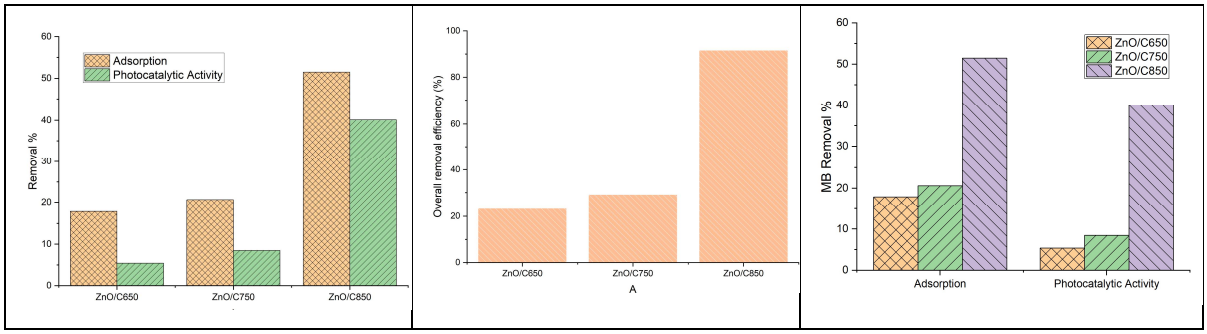

Figure 17: (a) Comparison of adsorption and photocatalytic capacities for each ZnO/C composites (b) Overall removal efficiency for ZnO/C650, ZnO/C750 and ZnO/C850 (c) Comparison between adsorption and photocatalytic degradation capacities of ZnO/C composites

For ZnO/C850, it was found that there was a good initial absorbance of 51.49 % in dark and then a gradual decrease in absorbance was observed at stirring under UV, reaching removal efficiency of 91.58 % at 120 minutes showing both significant adsorption by carbon matrix during stirring in the dark and photocatalytic activity by ZnO under UV irradiation. While the adsorptive capacity was 51.49%, photocatalytic efficiency was also large i.e. 40.09%. This shows high temperature carbonization is conducive for increment in both adsorptive capacity and photocatalytic activity.

Bar graph depicted in

Figure 17 *(a) compares the adsorption capacities and photocatalytic capacities of each ZnO/C composites separately where we observe that while both adsorption capacity and photocatalytic capacities increase slightly with increase in carbonization temperature from 650˚C to 750˚C, they increase drastically at 850˚C. Similarly, the bar graph in*

Figure 17*(c) compares the adsorption and photocatalytic capacities of each composite individually where we see that for each composite adsorption capacity is significantly higher than photocatalytic capacity. Bar chart in*

Figure *17*(b) clearly shows that ZnO/C850 has the highest removal efficiency of 91.58 % among the three composites.

In previous studies as well, it was found that high carbonization temperature allows for increased adsorption of MB onto the carbon matrix surface as well as higher photocatalytic degradation activity by ZnO (Hu et al., 2020), (Zhang et al., 2010), (Bakri et al., 2026). Higher temperature carbonization in ZnO-carbon composites results in creation of more mesopores and macropores in the carbon matrix as the volatiles vaporize, thereby increasing surface area

drastically (Zhang et al., 2010). At lower temperatures, carbonization of the Zn incorporated biomass is incomplete. Though this preserves the oxygen rich functional groups that can promote binding of MB dye to the carbon matrix, the formation of mesopores and macropores is hindered (de Moraes et al., 2019). Also, lower temperature carbonization results in predominantly amorphous carbon matrix as demonstrated by the XRD analysis in Section. Lower graphitization means π - π stacking of MB onto the carbon matrix becomes less, lowering contact. This explains the lower adsorption seen in ZnO/C650 and ZnO/C750 samples as compared to ZnO/C850. Less graphitization will also lower the conductivity of the carbon matrix. So, electrons generated at the ZnO sites during UV irradiation cannot be effectively transferred elsewhere quickly enough. It will prevent efficient charge separation causing electron-hole pair to recombine quickly. This considerably reduces the capacity of ZnO to form ROS under UV irradiation (Bakri et al., 2026) as confirmed by nominal photocatalytic activity seen in ZnO/C650 and ZnO/750 compared to ZnO/C850. The ZnO/C650 and ZnO/C750 samples could not break down the MB chromophores because ROS generation was hampered by quick electron-hole pair recombination as the carbon matrix was unable to pull the electrons away from holes. This shows at least partial graphitization of the carbon matrix is essential for ZnO-carbon composite to show significant photocatalytic activity.

4.3 Study of reaction kinetics

The adsorption and photocatalytic degradation of MB dye by the three samples ZnO/C650, ZnO/C750 and ZnO/C850 was also compared using a plot of C/C0 vs time as shown in **Figure *18***.

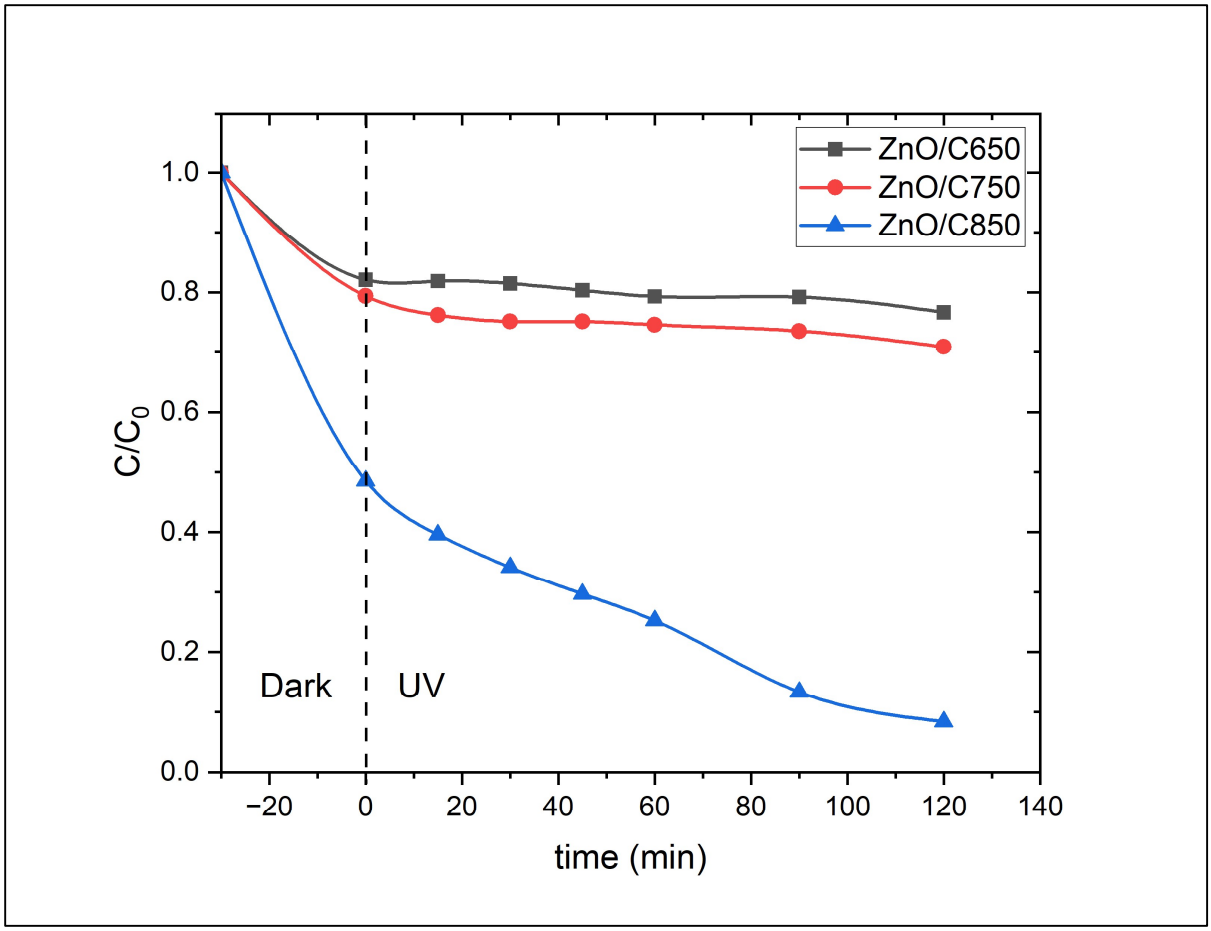

Figure 18: A plot of C/C0 vs time for ZnO/650, ZnO/750 and ZnO/850

From the graph in **Figure *18*** it is clearly visible that ZnO/C 850 sample has the best performance among them all. After the initial adsorption of MB dye, C/C0 for the ZnO/C650 composite remains almost constant from the beginning of UV irradiation process while in ZnO/C750 composite concentration slightly lowers due to some photocatalytic activity in the initial stage of UV irradiation and after that it plateaus with very little change. However, in ZnO/C850 composite, after initial adsorption phase, concentration of MB dye continues to decrease almost linearly. This behaviour of the composites carbonized at different temperatures can be summarized using a bar diagram as shown in **Figure *19***.

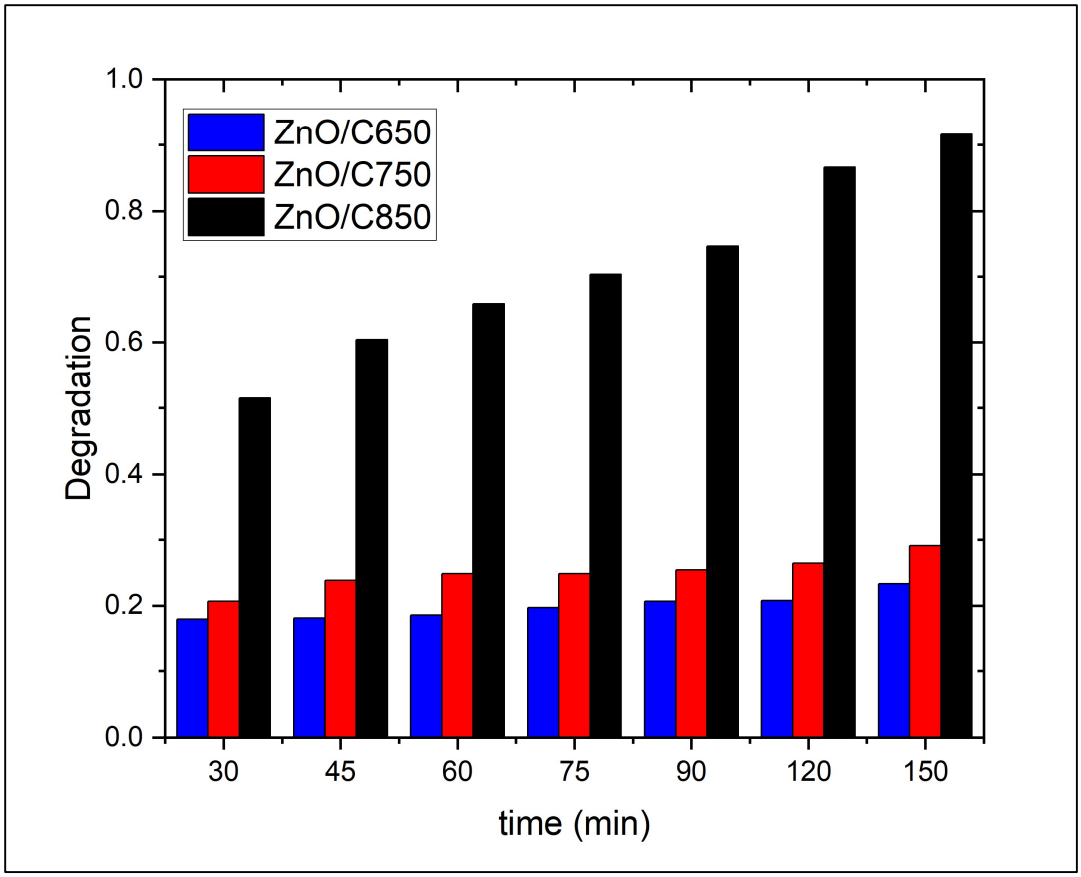

Figure 19: Behaviour of the composites carbonized at different temperatures

To explain the above seen behaviour of the composites, we must understand how the adsorption and degradation kinetics progresses and which mechanism it follows. This can be done by the help of various reaction kinetics models. Therefore, the pseudo first order model (Langmuir-Hinshelwood model) and pseudo second order model, as given by equations (4) and (5) respectively, were studied.

The pseudo first order Langmuir-Hinshelwood model was fitted for the adsorption and dye degradation by the composites ZnO/C650, ZnO/C750 and ZnO/C850 respectively using the equation (4) as given below.

$$\ln\left(\frac{C}{C_0}\right) = -kt$$

A plot of ln (C/C0) vs t must fit in a straight line with high correlation coefficient value, R^2 for the reaction to follow pseudo first order model. **Figure *20*** shows the fitted plot obtained for all three composite samples for the pseudo first order reaction model.

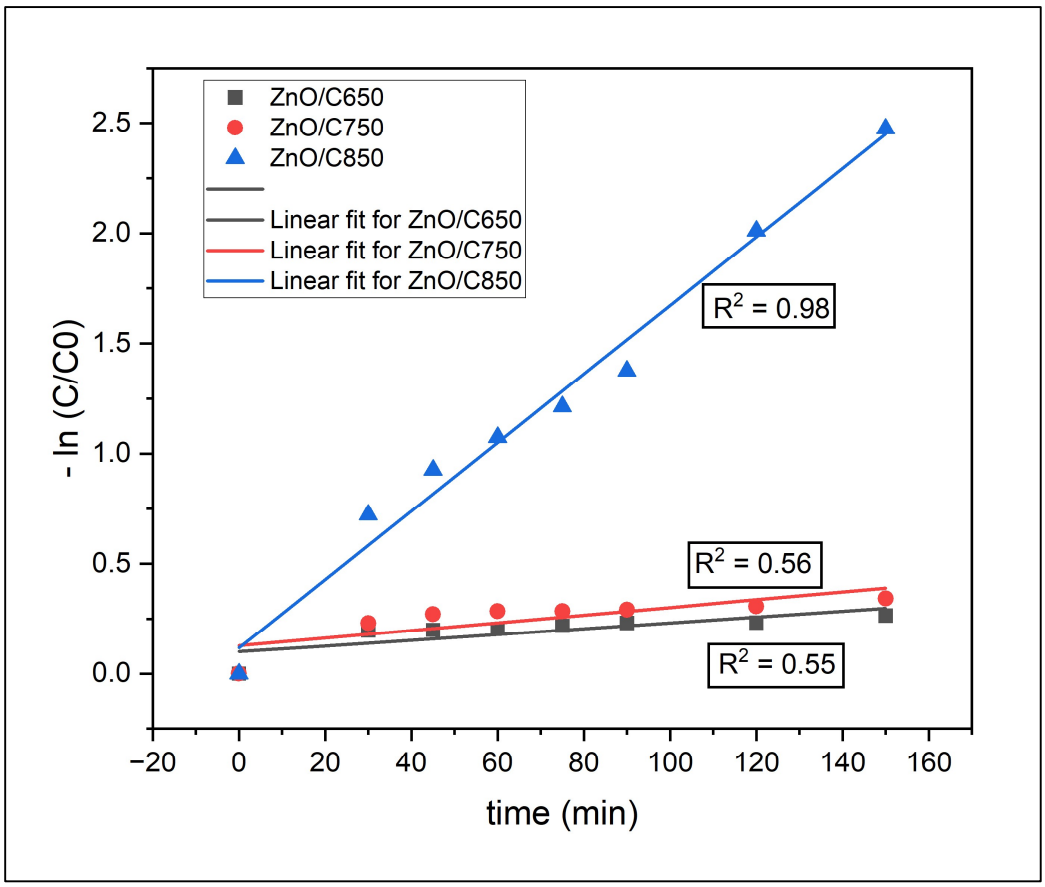

Figure 20: Plot for all composite samples for pseudo first order reaction model

The rate constant (k) and R^2 values for each ZnO/C composite for the pseudo first order reaction kinetics model are listed in **Table *5*** below:

Table 5 : Fitted R^2 and rate of reaction, k obtained for pseudo first order model

	Rate of reaction, k (min^{-1})	**R^2**
ZnO/C650	0.00131	0.55
ZnO/C750	0.00174	0.56
ZnO/C850	0.01555	0.98

The rate of reaction i.e. rate constants for ZnO/C650, ZnO/C750 and ZnO/C850 were obtained as 0.00131 min-1, 0.00174 min-1 and 0.01555 min-1 respectively which shows reaction is much faster in ZnO/C850 compared to the other two composites. This has already been validated by the good overall removal efficiency shown by ZnO/C850 as presented in **Error! Reference source not found.** . The R^2 values of 0.55, 0.56 and 0.98 were obtained for ZnO/C650, ZnO/C750 and ZnO/C850 respectively which means pseudo first order reaction model does not fit well suggesting the adsorption and degradation kinetics of MB degradation by the ZnO/C composites does not follow pseudo first order reaction strictly. This implies that adsorption and photocatalytic degradation process are not simple diffusion - dominated process, and there must be other factors involved in determining the rate of reaction.

Pseudo second order reaction kinetics model as given by

$$\frac{t}{q_t} = \frac{1}{k_2 q_e^2} + \frac{t}{q_e}$$

was also fitted for the adsorption and photocatalytic degradation of MB dye by the ZnO/C composites. Plot of t/q_t vs t was linearly fitted to obtain equilibrium capacity, q_e and and second order rate constant, k_2.

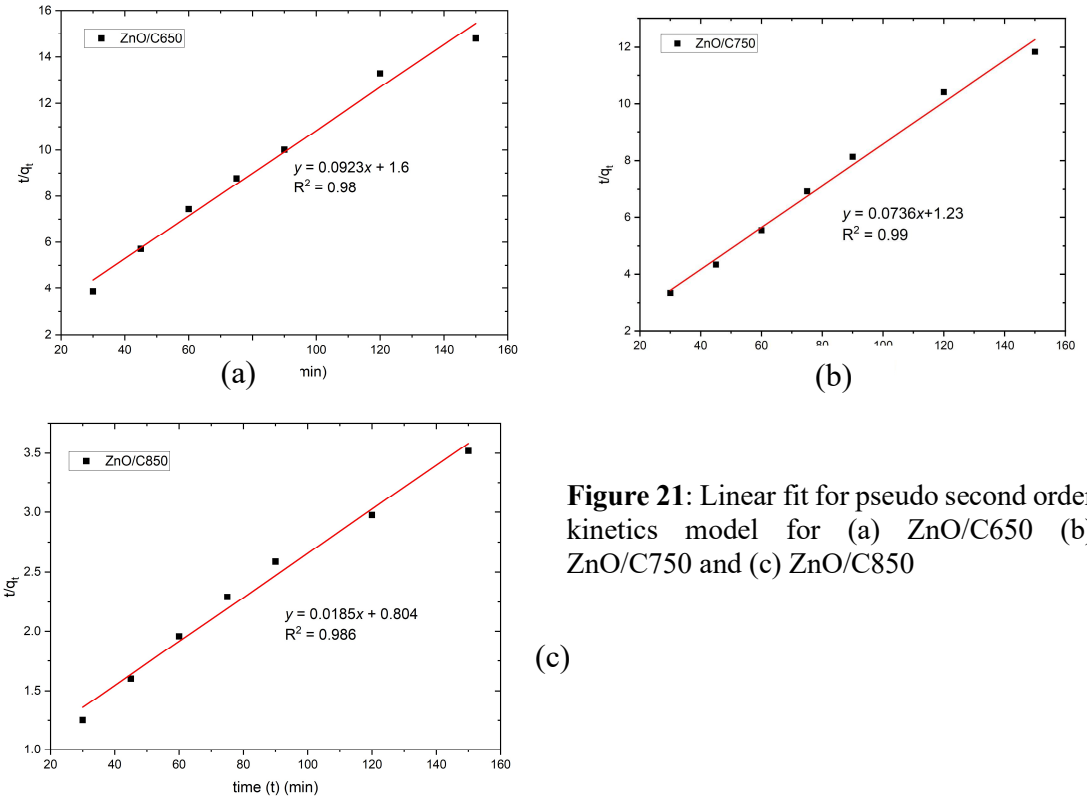

Figure 21: Linear fit for pseudo second order kinetics model for (a) ZnO/C650 (b) ZnO/C750 and (c) ZnO/C850

The equilibrium capacity (q_e), second order rate constant (k_2) and correlation coefficient, R^2 values obtained from the linear fit plots in **Figure *21*** (a), (b) and (c) are listed in the below in **Table *6***.

Table 6 : Equilibrium capacity (q_e), rate constant(k_2) and fitted R^2 values for pseudo second order reaction for the ZnO/C composites

	q_e (mg/g) (experimental)	q_e (mg/g) (calculated)	k_2 (g/mg min)	R^2
ZnO/C650	10.15	10.83	0.0053	0.98
ZnO/C750	12.65	13.58	0.0044	0.99
ZnO/C850	42.06	53.99	0.000427	0.986

We see that the correlation coefficient, R^2 values for ZnO/C650, ZnO/C750 and ZnO/C850 are 0.98, 0.99 and 0.986 respectively, all of which are very close to 1. Similarly, the experimental and calculated equilibrium capacities (q_e) for ZnO/C650 and ZnO/C750 composites are in good agreement with each other which demonstrates that the MB dye adsorption and degradation by the as-obtained ZnO/C composite samples follow pseudo second order reaction kinetics. This indicates that chemisorption of the MB dye molecule onto the adsorbate composite's surface through sharing or exchange of electrons between them is the dominant mode of adsorption. The calculated q_e for ZnO/C850 is also in a close range to the experimental q_e suggesting chemisorption also occurs in it. Also, the higher value of equilibrium capacity q_e for ZnO/C850 as compared to other two samples suggests that ZnO/C850 has larger number of active sites that help in faster uptake of the dye by the adsorbent surface.(Darweesh et al., 2026). It should be noted that ZnO/C850 fits both pseudo first order and pseudo second order reaction kinetics models which is commonly seen in bifunctional materials that show both adsorption as well as photocatalytic degradation. This is because firstly both diffusion and chemisorption can compete during adsorption of the dye. Secondly, the dye adsorbed on the surface is being constantly degraded clearing the sites for more adsorption. Also, during degradation of MB dye, intermediates can be formed which can compete with the MB dye for the active sites. So, there is no clear single rate-limiting factor, thus allowing multiple models to fit well (Ali et al., 2026).

To conclude, it was found that the performance of ZnO/C composites synthesized by carbonization of ZIF-8 impregnated azolla biomass template is highly dependent on carbonization temperature. Sample carbonized at higher temperature of 850˚C, ZnO/C850 gave good results while the composites prepared at lower carbonization temperatures ZnO/C650 and ZnO/C750 performed poorly. The FeSEM image analysis, FTIR analysis, XRD analysis and reaction kinetics studies performed on the composites all strongly validated each other and also validate the performance of the composites in MB dye adsorption and degradation. This study compares well with other similar studies done using MB on dye degradation under similar conditions. This demonstrates that the ZnO/C composites prepared through this simple method using water as green solvent on an abundant and locally available cheap biomass source *Azolla pinnata* is a viable approach towards developing ecofriendly and eco-smart materials to be used for wastewater treatment. Below is given a list of some studies done on photocatalytic degradation of MB dye to which this study compares to well enough.

Table 7: Comparison study of photocatalytic degradation of MB dye by various composites

Biomass/ Precursor	**Composite type**	**Dye**	**Degradation Result**	**Author (s)**
Indian Jujube (500 ˚C, 3hr)	ZnO/AC	MB	97.25% in 2 hrs (UV)	Kumari (2022)
Graphene oxide	TiO_2/GO (20%)	MB	97.5% in 35 min dark + 140 min in visible light	(Wang et al., 2019)
ZIF-8 (800˚C, 1hr)	ZnO/C	MB	70 % in visible light	(Hussain et al., 2019)
ZIF-8 on azolla (850 ˚C)	**ZnO/C**	**MB**	**91.58 % 10 mg / 50 mL (10 ppm) in UV, 2 h**	**Present study**

CHAPTER 5. CONCLUSIONS

Azolla pinnata, a readily available, nitrogen rich biomass was decorated with ZIF-8 as sacrificial template in a simple and eco-friendly manner using water as a green solvent and was then carbonized in inert N_2 atmosphere at three different temperatures of 650˚C, 750˚C and 850˚C to synthesize ZnO incorporated carbon composites. The morphology and composition of the composites were studied using FeSEM/EDX, FTIR and XRD. The photocatalytic performance of the as-synthesized ZnO/carbon composites were then studied via adsorption and degradation of MB dye in aqueous solution by these composites at ambient neutral (pH 7) conditions in dark and under UV light respectively. The major conclusions of this study are listed below:

- From FeSEM image, it was found that the ZIF-8 crystallites of flattened and elongated hexagonal shape grew uniformly on the azolla substrate which upon carbonization changed into fine beads dispersed uniformly over the substrate which when analyzed by EDX showed in total 11.33% zinc was dispersed evenly on the composite.
- FTIR confirmed the formation of ZnO/carbon composites and XRD showed the formation of ZnO NPs embedded on the carbon matrix. The composite carbonized at higher temperature of 850 ˚C showed better graphitization of carbon matrix and higher crystallinity of ZNO NPs than the other two samples.
- Consequently, the composite carbonized at 850 ˚C performed best with 91.58% removal efficiency for 10 ppm MB dye (10 mg of composite in 50 mL solution). The other two composites performed poorly.
- Poor performance of composites carbonized at lower temperature of 650˚C and 750˚C was attributed firstly, to absence of hierarchical pores in their carbon matrix due to insufficient carbonization due to which diffusion assisted uptake of MB dye did not become feasible and secondly, due to lack of graphitized regions because of which electron-hole recombination could not be prevented.
- Best degradation performance by the composite carbonized at 850˚C can be explained along similar lines. Higher temperature carbonization allowed formation of hierarchical pores for diffusion assisted adsorption of MB dye and the presence of turbostratic

graphitic regions allowed both chemisorption of MB dye molecules as well as fast electron transport which prevented electron-hole recombination.

- Both pseudo first order (Langmuir-Hinshelwood) and pseudo second order reaction kinetics were studied for the three composites. Lower temperature composites (carbonized at 650˚C and 750˚C) were found to obey only pseudo second order reaction kinetics implying lack of diffusion assisted adsorption and presence of only chemisorption due to functional groups present on the surface. Higher temperature (850˚C) composite was found to follow both pseudo first order and pseudo second order reaction kinetics which is common for bifunctional materials where adsorption by diffusion, chemisorption and photodegradation compete for active sites.
- Finally, the performance of the as synthesized azolla derived ZnO/carbon composite was compared with other similar studies. On the whole, azolla biomass derived ZnO/carbon composite shows promise as an effective, sustainable, low-cost and multifunctional material for wastewater treatment.

6. RECOMMENDATIONS/FUTURE WORKS

Due to time constraint important other tests and analyses could not be performed on the synthesized ZnO-carbon composite which should carried out in future.

1. Study on recovery and reusability if the ZnO/carbon composite must be done in future.

2. Study of types of ROS involved and hence the reaction mechanism of the photocatalytic degradation of MB dye can be ascertained using various scavengers.

3. Effect of pH on the adsorption and photodegradation should be studied.

4. Effect of various common anions like nitrate, sulphate and chloride in the aqueous solution of the dye can also be studied so that it more closely resembles real scenario of waste water.

5. Effect of ZnO/carbon composite on various microbial pathogens upon UV irradiation can be studied.

6. Feasibility of cleaning water of various toxic heavy metal ions by the composite can also be studied.

REFERENCES

Akinbile, C. O., Ogunrinde, T. A., Che bt Man, H., & Aziz, H. A. (2016). Phytoremediation of domestic wastewaters in free water surface constructed wetlands using Azolla pinnata. *International journal of phytoremediation*, *18*(1), 54-61.

Akir, S., Hamdi, A., Addad, A., Coffinier, Y., Boukherroub, R., & Omrani, A. D. (2017). Facile synthesis of carbon-ZnO nanocomposite with enhanced visible light photocatalytic performance. *Applied Surface Science*, *400*, 461-470.

Al-Nuaim, M. A., Alwasiti, A. A., & Shnain, Z. Y. (2023). The photocatalytic process in the treatment of polluted water. *Chemical papers*, *77*(2), 677-701.

Ali, K., Sethi, P., & Basu, S. (2026). ZIF-67/CQD nanohybrids for combined adsorptive and photocatalytic removal of tetracycline: kinetic, isotherm, and mechanistic insights. *RSC Sustainability*.

Amin, M. T., Alazba, A. A., & Manzoor, U. (2014). A review of removal of pollutants from water/wastewater using different types of nanomaterials. *Advances in materials science and engineering*, *2014*(1), 825910.

Andriantsiferana, C., Mohamed, E. F., & Delmas, H. (2014). Photocatalytic degradation of an azo-dye on TiO2/activated carbon composite material. *Environmental technology*, *35*(3), 355-363.

Asian Development Bank, I. (2021). *Johkasou – Wastewater Management in a Local Municipality in Japan*. https://www.adb.org/publications/johkasou-wastewater-management-japan

Bakri, R., Bozetine, H., Aziri, S., Djebra, Y., Berkane, N., Aberkane, D., Hadjersi, T., & Amrane, A. (2026). Microwave synthesis of green ZnO/carbon nanocomposite with enhanced photocatalytic activity under UV and solar light. *Journal of the Chinese Chemical Society*, *73*(2), 350-365.

Bekele, T., & Alamnie, G. (2025). The photocatalytic degradation of organic pollutants-a comprehensive overview. *Results in Chemistry*, 102758.

Bergaoui, M., Khalfaoui, M., Awadallah-F, A., & Al-Muhtaseb, S. (2021). A review of the features and applications of ZIF-8 and its derivatives for separating CO2 and isomers of C3-and C4-hydrocarbons. *Journal of Natural Gas Science and Engineering*, *96*, 104289.

Bodzek, M., Konieczny, K., & Kwiecińska-Mydlak, A. (2020). Nanotechnology in water and wastewater treatment. Graphene–the nanomaterial for next generation of semipermeable membranes. *Critical reviews in environmental science and technology*, *50*(15), 1515-1579.

Cary, P. R., & Weerts, P. G. (1992). Growth and nutrient composition of Azolla pinnata R. Brown and Azolla filiculoides Lamarck as affected by water temperature, nitrogen and phosphorus supply, light intensity and pH. *Aquatic Botany*, *43*(2), 163-180.

Chander, S., Lodha, A., Veer, K., & Gupta, A. (2024). Enhanced methylene blue dye sequestration by carbon-embedded mesoporous zinc oxide nanoparticles fabricated utilizing Aloe barbadensis miller biowaste: Batch optimization, simulation modeling, and textile effluent feasibility. *Materials Today Communications*, *40*, 110107.

Chen, X., Song, X., Chen, W., Ao, T., Yang, Q., & Zhao, L. (2025). MOFs/biomass-derived carbon as a high-performance anode for phosphorus removal. *Separation and Purification Technology*, *354*, 129125.

Cheng, S., Zhang, L., Xia, H., Zhang, S., Peng, J., & Wang, S. (2016). Crofton weed derived activated carbon by microwave-induced KOH activation and application to wastewater treatment. *Journal of Porous Materials*, *23*(6), 1597-1607.

Cruz, G., Gómez, M., Solis, J., Rimaycuna, J., Solis, R., Cruz, J., Rathnayake, B., & Keiski, R. (2018). Composites of ZnO nanoparticles and biomass based activated carbon: adsorption, photocatalytic and antibacterial capacities. *Water Science and Technology*, *2017*(2), 492-508.

Cui, N., Bi, K., Sun, W., Wu, Q., Li, Y., Xu, T., Lv, B., & Zhang, S. (2021). Effect of pyrolysis conditions on the performance of Co–doped MOF–derived carbon catalysts for oxygen reduction reaction. *Catalysts*, *11*(10), 1163.

Darabdhara, J., Hazarika, B., & Ahmaruzzaman, M. (2026). Zn-based metal organic frameworks encapsuated cauliflower leaves-derived biochar composite for photocatalytic removal of victoria blue and crystal violet. *Scientific Reports*.

Darweesh, R. F., Zaki, R. M., Mahdy, A., & Ahmed, A. S. (2026). Enhanced adsorption of methylene blue (MB) dye by the MoS 2/ZIF-8 composite: isotherm and kinetics studies. *Materials Advances*, *7*(1), 338-350.

Epelle, E. I., Okoye, P. U., Roddy, S., Gunes, B., & Okolie, J. A. (2022). Advances in the applications of nanomaterials for wastewater treatment. *Environments*, *9*(11), 141.

Eswaran, P., Madasamy, P. D., Pillay, K., & Brink, H. (2025). Sunlight-driven photocatalytic degradation of methylene blue using ZnO/biochar nanocomposite derived from banana peels. *Biomass Conversion and Biorefinery*, *15*(8), 12347-12367.

Gao, M., Lu, M., Zhang, X., Luo, Z., & Xiao, J. (2022). Application of fiber biochar–MOF matrix composites in electrochemical energy storage. *Polymers*, *14*(12), 2419.

Hu, C., Hu, X., Li, R., & Xing, Y. (2020). MOF derived ZnO/C nanocomposite with enhanced adsorption capacity and photocatalytic performance under sunlight. *Journal of hazardous materials*, *385*, 121599.

Hussain, M. Z., Pawar, G. S., Huang, Z., Tahir, A. A., Fischer, R. A., Zhu, Y., & Xia, Y. (2019). Porous ZnO/Carbon nanocomposites derived from metal organic frameworks for highly efficient photocatalytic applications: A correlational study. *Carbon*, *146*, 348-363.

Hussain, M. Z., Schneemann, A., Fischer, R. A., Zhu, Y., & Xia, Y. (2018). MOF derived porous ZnO/C nanocomposites for efficient dye photodegradation. *ACS Applied Energy Materials*, *1*(9), 4695-4707.

Ilhami, F. B., Mozef, T., Wihadi, M. N. K., Khasanah, M., Putri, N. P., Kusumawati, D. H., Kao, C.-Y., Kuo, D.-H., & Gultom, N. S. (2024). Developing zinc oxide and peanut shell-derived carbon star-shaped composite materials for effective photo-antibacterial treatment. *Heliyon*, *10*(12).

Isai, K. A., & Shrivastava, V. S. (2019). Photocatalytic degradation of methylene blue using ZnO and 2% Fe–ZnO semiconductor nanomaterials synthesized by sol–gel method: a comparative study. *SN Applied Sciences*, *1*(10), 1247.

Jayasundara, P. (2022). Wastewater Treatment by Azolla: A review. *Diyala Agricultural Sciences Journal*, *14*, 45-51. https://doi.org/10.52951/dasj.22140105

Jian, M., Liu, B., Liu, R., Qu, J., Wang, H., & Zhang, X. (2015). Water-based synthesis of zeolitic imidazolate framework-8 with high morphology level at room temperature. *RSC Advances*, *5*(60), 48433-48441.

Jing, H.-P., Wang, C.-C., Zhang, Y.-W., Wang, P., & Li, R. (2014). Photocatalytic degradation of methylene blue in ZIF-8 [10.1039/C4RA08820D]. *RSC Advances*, *4*(97), 54454-54462. https://doi.org/10.1039/C4RA08820D

Karki, B. K., Baniya, S., Kharel, H. L., Angove, M. J., & Paudel, S. R. (2024). Urban wastewater management in Nepal: generation, treatment, engineering and policy perspectives. *H2Open Journal*, *7*(2), 222-242.

Khan, I., Saeed, K., Zekker, I., Zhang, B., Hendi, A. H., Ahmad, A., Ahmad, S., Zada, N., Ahmad, H., & Shah, L. A. (2022). Review on methylene blue: its properties, uses, toxicity and photodegradation. *Water*, *14*(2), 242.

Kordbacheh, F., & Heidari, G. (2023). Water pollutants and approaches for their removal. *Materials Chemistry Horizons*, *2*(2), 139-153.

Kouser, S., Hezam, A., Khadri, M., & Khanum, S. (2022). A review on zeolite imidazole frameworks: synthesis, properties, and applications. *Journal of Porous Materials*, *29*. https://doi.org/10.1007/s10934-021-01184-z

Kumari, A. (2022). *Fabrication of Metal Oxide/Activated Carbon Nanocomposite from Jujube (Ziziphus Mauritiana) Seeds for Photodegradation of Dye* IOE Pulchowk Campus].

Lee, Y.-R., Jang, M.-S., Cho, H.-Y., Kwon, H.-J., Kim, S., & Ahn, W.-S. (2015). ZIF-8: A comparison of synthesis methods. *Chemical Engineering Journal*, *271*, 276-280.

Ma, B., Zhu, J., Xu, Y., Zhang, L., Liu, D., Chen, C., & Sun, B. (2025). Photocatalytic degradation of methylene blue using ZnO modified with nano-biochar derived from bacterial cellulose. *Ceramics International*, *51*(11), 14948-14956.

Maddu, A., Meliafatmah, R., & Rustami, E. (2021). Enhancing Photocatalytic Degradation of Methylene Blue Using ZnO/Carbon Dots Nanocomposite Derived From Coffee Grounds. *Polish Journal of Environmental Studies*, *30*(1).

Manna, M., & Sen, S. (2023). Advanced oxidation process: a sustainable technology for treating refractory organic compounds present in industrial wastewater. *Environmental Science and Pollution Research*, *30*(10), 25477-25505.

Mitiku, A. A. (2020). A review on water pollution: causes, effects and treatment methods. *Int J Pharm Sci Rev Res*, *60*(2), 94-101.

Möslein, A. F., Donà, L., Civalleri, B., & Tan, J.-C. (2021). Defects in ZIF-8 crystallization and their impact on mechanical properties. *arXiv preprint arXiv:2109.05557*.

Mutegoa, E. (2024). Efficient techniques and practices for wastewater treatment: an update. *Discover Water*, *4*(1), 69.

Ngullie, R. C., Bhuvaneswari, K., Shanmugam, P., Boonyuen, S., Smith, S. M., & Sathishkumar, M. (2022). Magnetically recoverable biomass-derived carbon-aerogel supported ZnO (ZnO/MNC) composites for the photodegradation of methylene blue. *Catalysts*, *12*(9), 1073.

Oladoye, P. O., Ajiboye, T. O., Omotola, E. O., & Oyewola, O. J. (2022). Methylene blue dye: Toxicity and potential elimination technology from wastewater. *Results in Engineering*, *16*, 100678.

Salah, W., Djeridi, W., Houas, A., & Elsellami, L. (2024). Synergy between activated carbon and ZnO: A powerful combination for selective adsorption and photocatalytic degradation. *Materials Advances*, *5*(4), 1667-1675.

Shahzadi, S., Akhtar, M., Arshad, M., Ijaz, M. H., & Janjua, M. R. S. A. (2024). A review on synthesis of MOF-derived carbon composites: innovations in electrochemical, environmental and electrocatalytic technologies. *RSC Advances*, *14*(38), 27575-27607.

Thi Luyen, N., Van Nguyen, K., Van Dang, N., Quang Huy, T., Hoai Linh, P., Thanh Trung, N., Nguyen, V.-T., & Thanh, D. V. (2023). Facile one-step pyrolysis of ZnO/biochar nanocomposite for highly efficient removal of methylene blue dye from aqueous solution. *ACS omega*, *8*(30), 26816-26827.

unwater.org. (7 April). *https://www.unwater.org/publications/progress-wastewater-treatment-2024-update* https://www.unwater.org/publications/progress-wastewater-treatment-2024-update

Wang, R., Shi, K., Huang, D., Zhang, J., & An, S. (2019). Synthesis and degradation kinetics of TiO2/GO composites with highly efficient activity for adsorption and photocatalytic degradation of MB. *Scientific Reports*, *9*(1), 18744.

Zghal, S., Jedidi, I., Cretin, M., Cerneaux, S., & Abdelmouleh, M. (2023). Adsorptive removal of Rhodamine B dye using carbon graphite/cnt composites as adsorbents: Kinetics, isotherms and thermodynamic study. *Materials*, *16*(3), 1015.

Zhang, C., Han, C., Sholl, D. S., & Schmidt, J. (2016). Computational characterization of defects in metal–organic frameworks: Spontaneous and water-induced point defects in ZIF-8. *The journal of physical chemistry letters*, *7*(3), 459-464.

Zhang, F., Lan, J., Yang, Y., Wei, T., Tan, R., & Song, W. (2013). Adsorption behavior and mechanism of methyl blue on zinc oxide nanoparticles. *Journal of Nanoparticle Research*, *15*. https://doi.org/10.1007/s11051-013-2034-2

Zhang, P., Shen, Z., Jia, L., & Qiu, J. (2026). Biomass-Derived Carbon for Boosting Photocatalysis. *Small*, *22*(8), e12210.

Zhang, Z., Niu, H., Fernández, Y., Menéndez, J., Peng, J., Zhang, Z., Zhang, L., & Duan, X. (2010). Effect of temperature on the properties of ZnO/activated carbon composites from spent catalysts containing zinc acetate. *Journal of the Taiwan Institute of Chemical Engineers*, *41*(5), 617-621.

Zhao, Y., Shi, J., Wang, X., Li, W., Wu, Y., & Jiang, Z. (2020). Biomass@ MOF-derived carbon aerogels with a hierarchically structured surface for treating organic pollutants. *Industrial & Engineering Chemistry Research*, *59*(39), 17529-17536.

Zhu, X., Zeng, Y., Zhao, X., Liu, D., Lei, W., & Lu, S. (2025). Biomass-derived carbon and their composites for supercapacitor applications: sources, functions, and mechanisms. *EcoEnergy*, *3*(3), e70000.